Long-term analysis of Formaldehyde by using Stationary, Mobile and Satellite observations over Pakistan

By

Tooba Zainab

00000172848

Institute of Environmental Science and Engineering (IESE)

School of Civil and Environmental Engineering (SCEE)

National University of Sciences and Technology (NUST)

Islamabad, Pakistan

(2019)

Long-term analysis of Formaldehyde by using Stationary, Mobile and Satellite observations over Pakistan

By

Tooba Zainab

(00000172848)

A thesis submitted in partial fulfillment of the requirements for the degree of

Master of Science

In

Environmental Sciences

Institute of Environmental Sciences and Engineering (IESE) School of Civil and Environmental Engineering (SCEE) National University of Sciences and Technology (NUST) Islamabad, Pakistan (2016)

THESIS ACCEPTANCE CERTIFICATE

It is certified that the contents and forms of the thesis entitled "Long-term analysis of Formaldehyde by using Stationary, Mobile and Satellite observations over Pakistan" submitted by Tooba Zainab (Reg # 172848) has been found satisfactory for the requirements of the degree of Master of Science in Environmental Science.

Supervisor: _____

Dr. M. Fahim Khokhar

Professor

IESE, SCEE, NUST

Head of Department: _____

Dr. Muhammad Arshad

Associate Professor

IESE, SCEE, NUST

Principal: _____

Dr. Tariq Mahmood

SCEE, NUST

CERTIFICATE

It is certified that the contents and form of the thesis entitled

“Long-term analysis of Formaldehyde by using Stationary, Mobile and Satellite observations over Pakistan”

Submitted by

Tooba Zainab

has been found satisfactory for the requirement of the degree

Supervisor: _____

Dr. Muhammad Fahim Khokhar

Professor

IESE, SCEE, NUST

Member: _____

Dr. Zeeshan Ali Khan

Associate Professor

IESE, SCEE, NUST

Member: _____

Dr. Sofia Baig

Assistant Professor

IESE, SCEE, NUST

DEDICATION

This work is dedicated to my loving parents,

Syed Shah Sharef and Firdous Fatima,

whose endless efforts, prayers and sacrificial care made it possible for me to complete this work.

ACKNOWLEDGEMENTS

All praise to Allah Almighty for giving us the blessing of Wisdom.

This dissertation would not have been possible without the guidance and the help of several individuals who, in one way or another, contributed in the preparation and completion of this study.

First and foremost, I would like to express my gratitude to my supervisor ***Dr. Muhammad Fahim Khokhar*** *for the comments, remarks, engagement and positive criticism through the learning process of this master thesis. Furthermore, many thanks to* ***Dr. Muhammad Zeeshan Ali Khan*** *and* ***Dr. Sofia Baig*** *who had always been very considerate and supportive in my research work.*

I am grateful to the staff of ***IESE, NUST*** *as they were very helpful and supportive.*

I am grateful to all members of CCARGO for being cooperative and helpful and special thanks to ***Mr. Muhammad Ahmed Subhani, Mr. Hafiz Ahsen Mehmood, Mr. Assadullah Shoaib and Miss Naila Zeb.***

I would also like to extend my thanks to all of my friends, well-wishers and loved ones who gave me support, without whose support and understanding it would have taken a much longer time to finish this work.

Special thanks to my parents and my siblings especially my brother ***Syed Azadar Hussain*** *for their consistent encouragement and endless support.*

Tooba Zainab

Table of Contents

LIST OF TABLES

LIST OF FIGURES

LIST OF ABBRIVEATIONS

HCHO	Formaldehyde
IESE- NUST	Institute of Environmental Sciences and Engineering - National University of Sciences and Technology
SOA	Secondary Organic Aerosols
µg/m^3	Microgram per Cubic meter
AMF	Air Mass Factor
ArcGIS	Arc Geographic Information System
DOAS	Differential Optical Absorption Spectroscopy
DOASIS	Differential Optical Absorption Spectroscopy Intelligent System
DSCD	Differential Slant Column Densities
MAX-DOAS	Multi-axis Differential Optical Absorption Spectroscopy
OMI	Ozone Monitoring Instrument
WHO	World Health Organization
WinDOAS	Windows Differential Optical Absorption Spectroscopy
VOCs	Volatile Organic Compounds
RMS	Root Mean Square
ppb	Parts per Billion

Abstract

Formaldehyde (HCHO) is an organic carbonyl compound found abundantly in the atmosphere. It is formed as a byproduct in the degradation pathways of many VOCs. This study was specifically designed to monitor the HCHO concentrations in different parts of Pakistan. Mini MAX-DOAS (Multi-Axis Differential Optical Absorption Spectroscopy) instrument was used for both stationary and mobile monitoring of HCHO. Long term continuous monitoring of HCHO was performed at IESE, NUST, Islamabad for a period of four years. Apart from that, mobile field campaigns in the megacities of Multan and Lahore were conducted. Also, HCHO concentration in various forest areas of Pakistan were measured to study the role forests in VOC production and consequent HCHO formation in the atmosphere. MAX-DOAS observations were used to measure the diurnal, daily and annual cycle of HCHO concentrations over IESE, Islamabad. The diurnal cycle showed a good correlation of 0.74 among HCHO concentrations and temperature data indicating that the concentration of HCHO increase with the increase in temperature. Moreover, the annual cycle showed highest concentration during summer followed by spring, autumn and winter. During field campaigns HCHO concentration was found to be maximum in the vicinity of Tea Garden, Shinkiari. It was observed that the concentration of HCHO in the forest areas was well below the threshold value of 83 ppbv given by World Health Organization (WHO). Field campaigns conducted in Multan and Lahore revealed that HCHO concentrations were comparatively higher than the forest areas and also exceeded the threshold value at some points. Furthermore, tropospheric HCHO VCDs derived from ground-based mini MAX-DOAS measurements were compared with

satellite data obtained from Ozone Monitoring Instrument (OMI). The satellite data underestimated the ground-based HCHO MAX-DOAS observations.

Chapter 1

1. Introduction

1.1. Background

Earth is the only planet in the solar system having a life supporting atmosphere (a thin layer of gases surrounding the earth). The earth's atmosphere not only provides us oxygen to breath but also has many other important roles to play. It acts as filter between the outer space and earth's surface by filtering out most of the harmful UV radiations. Through greenhouse effect, it also helps in keeping the earth temperature warm and to a greater extent prevents extreme daytime and nighttime temperature differences. Therefore, it is of our greatest interest to study the characteristics of the atmosphere, its composition, processes and response to various anthropogenic activities on both spatial and temporal scales.

Volatile organic compounds (VOCs) play crucial role in changing the composition of the atmosphere. They are emitted from both natural and anthropogenic sources. VOCs contribute in the formation of tropospheric ozone and secondary organic aerosols (SOAs). They can also impact the production of cloud condensation nuclei and influence the oxidization capacity of the atmosphere (Volker et al., 2006; Liakakou et al., 2007; Vrekoussis et al., 2010; Gouw et al., 2018).

1.2. Air Pollution in Pakistan

Air pollution has both natural and anthropogenic sources and poses severe threat to human health and environment. Fossil fuel combustion has significantly increased during the past decades and, is a major contributor of change in the atmospheric composition on global scale (Kampa & Castanas, 2008).

Pakistan is among the most populous countries in the world and there is a significant boom in the rate of urbanization, transportation, industrialization and energy production in the recent years (Colbeck et al., 2010). Continuous air quality monitoring stations are sparse in number and there is lack of proper air quality management in the country. Due to which Pakistan is suffering from deteriorated air quality.

1.3. Formaldehyde:

Formaldehyde (HCHO) is an important oxidization product of VOCs and act as tracer of VOC sources in the atmosphere. HCHO is highly ubiquitous in atmosphere and is attributed as the most abundant aldehyde in the atmosphere (Salthammer, 2013). It is produced by the photochemical degradation of methane and non-methane hydrocarbons (Stavrakou *et al.*, 2008; Chen et al., 2014). HCHO has both natural (vegetation) and anthropogenic (combustion of fossil fuels, industrial processes and biomass burning) sources (Ho et al., 2012; Lee et al., 1997; Hoque et al., 2018). However, it has a very short lifetime of only 2 hours (Palmer et al., 2003). The major sinks of HCHO are photolysis, wet deposition and oxidization by hydroxyl (OH) radicals (Vlasenko et al., 2010).

1.4. The Present Study:

This study basically comprises of the ground based and satellite monitoring of formaldehyde (HCHO) over Pakistan. Column densities of HCHO were measured by using Mini MAX-DOAS (Multi-Axis Differential Optical Absorption Spectroscopy) instrument mounted on the roof top of Institute of Environmental Sciences and Engineering, National University of Sciences and Technology, Pakistan. The Mini MAX-DOAS was also installed at different forest types in Pakistan for retrieval of HCHO data. Also, the HCHO column densities were quantified in the cities of Lahore and Multan by using CAR MAX-DOAS observations. The data retrieved from the instrument was then analyzed by using DOASIS software. Furthermore, the ground-based results were validated by satellite data.

1.5. Study Area:

Stationary monitoring of HCHO was carried out at NUST, Islamabad (lat:33.6479° N, lon:72.989638° E); Pine Park Hotel, Shogran, KPK (lat:34.6400471° N, lon:73.4640154° E); Pakistan Forest Institute field station, Shinkiari, KPK (lat:34.4724254° N, lon:73.2662724° E); National Tea Garden, Shinkiari, KPK (lat:34.45885° N, lon:73.2681623° E) ;Rama, Gilgit Baltistan (lat:35.3536335° N, lon:74.7982648° E); Bata Kundi, Gilgit Baltistan (lat:34.92994° N, lon:73.74858° E) and Deosai National Park, Gilgit Baltistan (lat:34.99522013° N, lon:75.2332428° E).

Also, mobile monitoring of HCHO was done in two metropolitan cities of Pakistan i.e. Multan (30.1984° N, 71.4687° E) and Lahore (lat:31.5546° N, lon:74.3572° E).

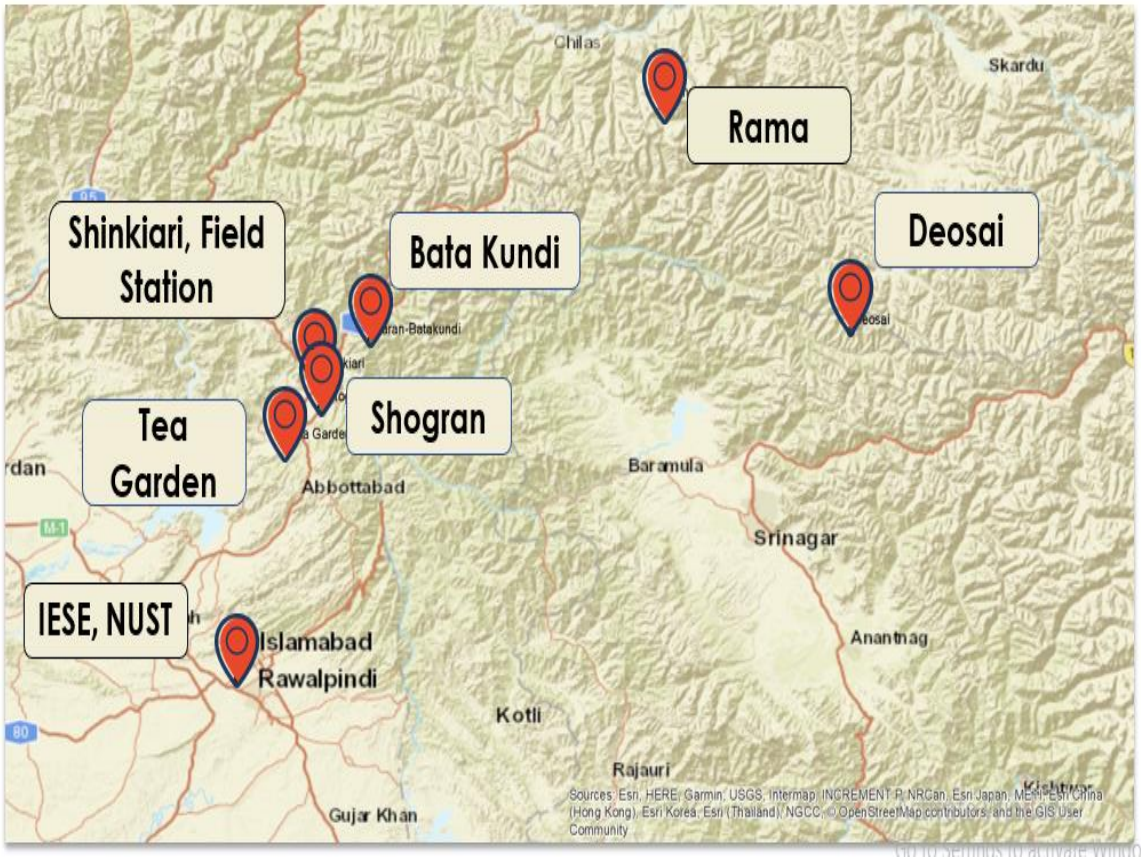

Figure 1:Map of Stationary HCHO monitoring sites selected for using MAX-DOAS instrument

1.6. Significance of the study:

Degradation of ambient air quality particularly in urban areas is a rapidly growing issue in Pakistan. The deteriorated air quality not only severely impacts the human health but also has its implications on the economy and environment of Pakistan. Pakistan's urban air quality is one of the worse in the South-Asian region. Industrial activities, agricultural burning and transportation are the major sources of air pollution in urban areas of Pakistan (Ali et al., 2006; Hussain, 2010; Khokhar et al., 2015).

This research will help in highlighting the severity and scope of air pollution in Pakistan with great emphasis on the importance of urgent need of abatement of air pollution in the country by the government and general public to improve Pakistan's air quality. By monitoring of formaldehyde in the urban areas of the country, the local sources of emissions of air pollutants will be identified and its possible impacts on human health and environment can be minimized. Forests, on the other hand, are considered to be responsible for the clean-up of atmosphere from pollutants but they also contribute to the deterioration of air quality by releasing Volatile Organic Carbons (VOCs) in the atmosphere (Simon et al., 2001; Nowak et al., 2014). This study not only identifies the anthropogenic sources of formaldehyde (HCHO) but also determines the biogenic sources of HCHO from different forest types of Pakistan. Pakistan lacks air quality monitoring stations and there is little emphasis on the monitoring of trace gases in the atmosphere (Khokhar et al., 2016). The data from this research can be used as a baseline by the concerned governmental departments, Non-Governmental Organizations (NGOs) and academic institutions for research, policy making and Air Quality Management (AQM) for the abatement of air pollution in the country.

1.7. Objectives of the Study:

The objectives of this study were:

1) Ground based monitoring of HCHO concentrations by using Max-DOAS (2015-2018).

2) Comparison of satellite observations for HCHO concentrations with ground based and car Max-DOAS observations over Pakistan.

Chapter 2

2. Literature Review

2.1. Atmospheric composition

Earth is surrounded by a thin layer of gases called the atmosphere. The thickness of this layer is reduced with the increase in altitude. There are different gasses in the atmosphere, some of them do not vary substantially both spatially and temporally while others are present in variable amounts, varying on hourly, daily, monthly and yearly basis. The gases in the atmosphere can be classified on the basis of their quantity and lifetime in the atmosphere. Nitrogen and Oxygen alone make up almost 99% of the dry atmosphere.

Gases like CO, N_2O, CH_4, O_3 and HCHO are present in very small amounts and are called trace gases. Trace gases accounts for approximately a 10^{th} of 1 percent of the atmosphere. The concentration of water vapors in the atmosphere varies from 0-4% of the atmosphere. It is higher in humid, tropical regions while lower in dry, arctic regions. Apart from gases, the atmosphere contains suspended particles called aerosols that originate mostly from natural sources (volcanic eruptions, biological materials, soil, sea salts and mineral dusts) and also has anthropogenic origin (incomplete combustion of fossil fuels, biomass burning and industrial particulates) (Ramanathan et al., 2001).

2.1.1. Trace Gases in the atmosphere

A large number of trace gases are present in the atmosphere like N_2O, CH_4, HCHO, NO_X, CO, SO_2 and O_3. Exponential increase in fossil fuel combustion, industrialization, automobiles, biomass burning and deforestation over the last 20 years has amplified the amount of trace gases in the atmosphere. It is an interesting fact that trace gases despite of their minute quantities, sometimes in less than one part per billion, contribute meaningfully in trapping outgoing infrared radiations. Many of the trace gases strongly absorb the infrared radiations and perturbates the earth's radiation energy balance, contributing to greenhouse effect and cause global warming (Dickinson & Cicerone., 1986).

HCHO is an active gas, in the presence of sunlight it can generate HO_2 free radicals by undergoing photolysis which in turn quickly reacts with NO to produce OH radical. OH radicals impacts the oxidation capacity of the atmosphere (Tian et al., 2018).

2.1.2. Volatile Organic Compounds (VOCs)

VOCs has a critical part in the overall chemistry of the troposphere. Major sources of VOCs include vegetation, biomass burning, fossil fuel combustion, industries, refineries, and consumer products (Fehsenfeld et al., 1992; Khan et al., 2000). In the presence of sunlight, VOCs in the troposphere reacts with nitrogen oxides resulting in the formation of photochemical smog. Ground level ozone (tropospheric ozone) is one of the major components of the photochemical smog (Marty et al., 2010).

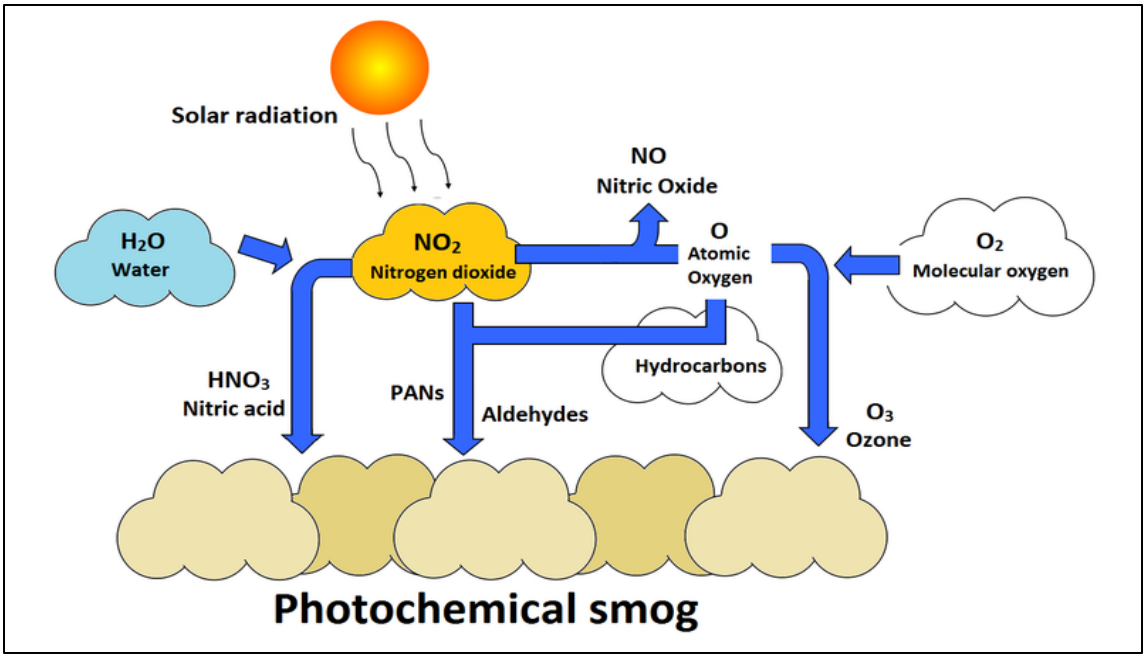

Figure 2. 1: Formation of photochemical smog (Miller et al., 2014).

Non-methane volatile organic compounds (NMVOCs) are vital precursors of the photochemical reactions causing the production of ozone and secondary organic aerosols (SOAs) (Wei et al., 2008). Non-methane volatile organic compounds (NMVOCs) are released into the atmosphere by both biogenic and anthropogenic emissions. But on a global scale the biogenic emissions (approximately 1150 Tg (C) per year) of NMVOCs exceed the anthropogenic emissions (approximately 100 Tg (C) per year) (Atkinson et al., 1997; Guenther et al., 1995). Biogenic NMVOC impacts ozone chemistry in various ways. Isoprene-one of the prominent NMVOC emitted from vegetation can play a part as a sink of oxidants, acting as sink for NO thus competing with ozone and can allow long distant transport of nitrogen, contributing to nitrogen sequestration (Guenther et al., 2000). The source of anthropogenic NMVOCs in the urban atmosphere is mainly vehicular emissions and refineries (Watson et al., 2001).

Amongst the organic atmospheric traces gases, methane (CH_4) is the most abundant one. Increased concentrations of methane contribute to perturbations in the atmosphere. CH_4 is a strong greenhouse gas (GHG). Although, CH_4 has a shorter lifetime in the atmosphere as compared to CO_2 but it has 21 times greater global warming potential (GWP) than CO_2 (Pachauri et al., 2008). In the polluted troposphere, due to its high reactivity, it gets oxidized by hydroxyl radicals (OH) and can form ozone, formaldehyde and carbon monoxide, in the presence of high concentrations of NOx (Wuebbles et al., 2002).

2.2. Formaldehyde (HCHO)

Formaldehyde is a highly reactive colorless gas with a strong smell. In the atmosphere, formaldehyde is not only released directly through anthropogenic and biogenic sources but is also produced by the oxidation of methane and non-methane VOCs which contributes about 70 to 90 percent of the total formaldehyde existing in the atmosphere (Palmer et al., 2003). It is an important trace gas as it is an intermediate in methane removal processes and the removal process of other hydrocarbons. In general, it impacts the overall chemical reactivity of the atmosphere.

2.2.1. Atmospheric chemistry of HCHO

Photochemical degradation pathways of various VOCs lead to the formation of formaldehyde in the atmosphere. The amount of HCHO in the atmosphere depends upon the season, location and time of the day. Methane is one of the major VOC contributing to higher HCHO concentrations in the atmosphere. Where there are lower concentrations of NOx in the atmosphere, formaldehyde is produced by the reaction of OH with methyl

peroxide in the methane oxidation process. In case of high concentrations of NOx in the atmosphere, methylperoxyl gets reduced by nitric oxide to methoxyl which further reacts with O_2 to produce HCHO (Equation 1-3) (Luecken et al., 2012).

$$CH_4 + OH + O_2 \rightarrow CH_3O_2^{\bullet} + H_2O \qquad \textbf{Eq. 1}$$

$$CH_3O_2^{\bullet} + NO \rightarrow CH_3O^{\bullet} + NO_2 \qquad \textbf{Eq. 2}$$

$$CH_3O^{\bullet} + O_2 \rightarrow HCHO + HO_2 \qquad \textbf{Eq. 3}$$

Isoprene is one of the most important biogenic VOC, having a very short lifetime and quickly oxidizes into formaldehyde by undergoing various atmospheric reactions (Sprengnether et al., 2002).

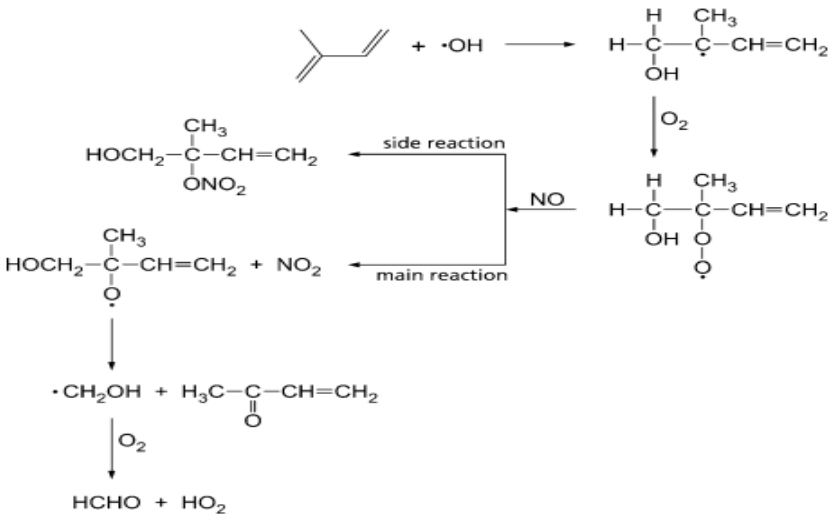

Figure 2. 2: Formation of HCHO from isoprene adopted from Salthammer, 2003

During the daytime, reaction with OH radicals and photolysis are the major loss processes of HCHO. Wet and dry deposition also removes HCHO from atmosphere. Also, at

nighttime HCHO is removed at slower rates from the atmosphere by reacting with nitrate radical (Wuebbles et al., 2002).

2.2.2. Sources of HCHO

The primary emission sources of HCHO in the atmosphere are fossil fuel combustion, forest fires, sea water, wood processing, plant and waste decay and biomass burning. The secondary sources of HCHO are photochemical oxidation of methane and non-methane VOCs in the atmosphere that are released into the atmosphere by industries, biomass burning, fossil fuel combustion, animals and vegetation (Li et al., 2014; Jones et al.,2009).

2.2.3. Sinks of HCHO

There are three major pathways by which HCHO is removed from the atmosphere i.e. removal via photolysis, OH oxidation and wet and dry deposition. The removal via photolysis is carried out through two pathways,

$$HCHO + hv \longrightarrow H2 + CO \qquad \textbf{Eq. 4}$$

$$HCHO + hv \longrightarrow H + HCO \qquad \textbf{Eq. 5}$$

While removal via OH oxidation takes place by reaction of OH radicals with HCHO (Cantrell et al.,1990),

$$HCHO + OH \longrightarrow HCO + H_2O \qquad \textbf{Eq. 6}$$

$$HCO + O_2 \longrightarrow HO_2 + CO \qquad \textbf{Eq. 7}$$

2.2.4. Health impacts of HCHO

Humans are exposed to formaldehyde by both outdoor and indoor environments and food. HCHO exposure leads to many adverse human health effects. Many cases of HCHO exposure from contaminated food, polluted water and air have been documented in the past two decades. Numerous such cases have raised public concern about health effects of HCHO exposure as these exposures have affected the human health negatively. Today the concern about HCHO health effects continues to grow worldwide due to the increased levels of exposure.

2.2.5. Acute effects

Irritation of throat, nose and eyes are the major effects of acute HCHO exposure. Human bodies come in contact with HCHO through ingestion, inhalation and via dermal exposure. It's acute exposure also causes chest pains, wheezing, coughing and bronchitis. Other effects include ulcer formation in mouth and stomach and also cause corrosion of gastrointestinal tract (Kim et al., 2011).

2.2.6. Chronic Effects

In humans, Chronic HCHO exposure via inhalation is responsible for causing irritation of nose, throat and eyes. When HCHO comes in contact with skin repeatedly in liquid form, it causes skin irritation and skin allergies (Tang et al., 2009).

Considering the effects on respiratory system of humans, a minimal risk level (MRL) concentration of 0.003 ppm has been assigned for HCHO chronic inhalation (Wilbur, 1999).

2.2.7. HCHO- A human carcinogen

HCHO has been ranked in Group B1 of chemicals by EPA and is a considered as a probable human cancer-causing agent (US Environmental Protection Agency, 1999). However, it was placed in Group 1 by International Agency for Research on Cancer (IARC) and was classified as human carcinogen later it was again assigned as B1 carcinogen. According to IARC HCHO is a nasopharyngeal cancer-causing agent (Baan et al., 2009).

2.3. DOAS Technique

Differential Optical Absorption Spectroscopy (DOAS) is a highly sensitive method used for identification and quantification of atmospheric species. This method is applicable for measurement of numerous atmospheric species for both local and global conditions. A basic DOAS setup consists of a source of light, fiber bundles for transfer of light to the instrument and a detector system including a telescope and spectrograph for recording of the absorption spectra.

2.3.1. Working Principle of DOAS

The working principle of DOAS is based on Beer-Lamberts Law,

$$I(\lambda) = I_0(\lambda)e^{-L\sigma(\lambda)n} \qquad \textbf{Eq. 8}$$

Where,

$I(\lambda)$: intensities measured

$I_0(\lambda)$: incoming radiation (reference intensities)

L: pathlength (cm)

$\sigma(\lambda)$: absorption cross sections (cm^2 $molecule^{-1}$)

n: number density of the species (molecules/cm3)

2.3.2. DOAS instrumentation

Both active and passive instrumentation can be used in DOAS technique. In both type of instrumentation, light source is required. Passive DOAS requires extraterrestrial light sources such as sun, star light or moon.

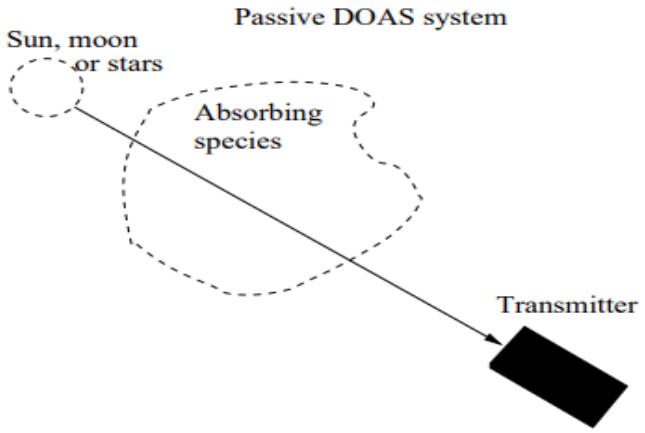

Figure 2. 3: Passive DOAS System (adopted from Brohede,2002)

While active DOAS requires lasers or thermal light sources apart from the extraterrestrial ones.

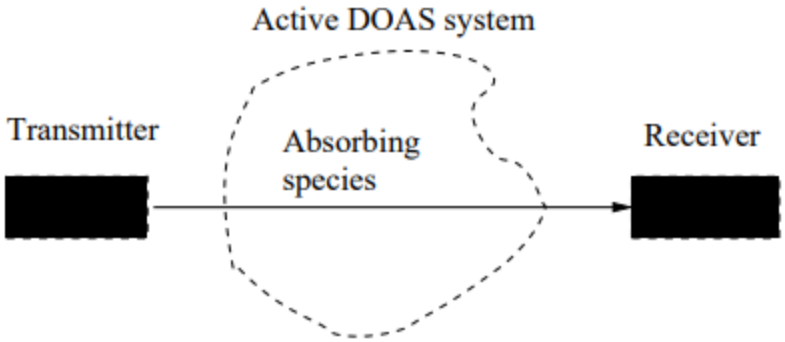

Figure 2. 4: Active DOAS System (adopted from Brohede,2002)

2.3.3. Atmospheric species measured by DOAS:

DOAS system detects atmospheric species that have narrow electronic transitions in the UV-visible region ranging from 300-800 nm. A number of species, for example, NO_2, HCHO, CHOCHO, O_3, SO_2, OClO and BrO can be measured by using DOAS setup.

2.3.4. Advantages of DOAS technique

DOAS is capable of measuring different atmospheric species simultaneously. Also, I_0 estimation is not required. Moreover, in case of DOAS technique Mie and Rayleigh scattering can be excluded. Due to long pathlengths, it is a highly sensitive technique (Hönninger et al. 2004).

2.3.5. Disadvantages of DOAS technique

In cloudy conditions and events such as rain and snow, the DOAS system fails to make measurements properly. Also, a confined number of atmospheric species have appropriate abortions in the UV-visible region (ISAC, 1994).

2.4. Ozone Monitoring Instrument

OMI consists of UV/VIS spectrometers that detects absorbed and scattered solar irradiance by the atmospheric constituents. It crosses the equator at 13:45 local afternoon time. In a single day OMI provides 14 orbits. For the retrieval of trace gases in UV/visible range in the atmosphere, OMI measures the solar irradiance spectrum and earth radiance. The radiance spectrum is normalized by solar irradiance spectrum to obtain reflectance spectrum. The reflectance spectrum is the main spectrum for atmospheric trace gas retrieval. OMI uses two channels of 0.5 nm spectral resolution (Levelt et al., 2006).

Chapter 3

3. Materials and Methods

3.1. Instrument-Mini MAX-DOAS

The instrument, Mini-MAX-DOAS was used in this research. Dimensions of this instrument are 13 cm × 19 cm × 14 cm and it has fully automatic functions. Specifically, it is used for the measurement of scattered sunlight. A quartz lens (40mm focal length) collects and focuses the light scattered by the sun into a spectrometer via optical cables. The spectrometer installed in the instrument have a spectral resolution of 0.7nm from Ocean Optics Inc. and model no is USB2000+ crossed Czerny-Tuner. It consists of a CCD-detector (one-dimensional) having spectral range of 320-465 nm recorded onto it and have 2048 pixels. A stepper motor is used for adjusting the viewing direction of the instrument at desired elevation viewing angles with a precision of 0.1 degree/step and 784Hz frequency. For maintaining a stable temperature, the spectrometer was cooled by using Peltier cooling system. All functions of the instrument were controlled by a computer system (windows XP installed) via USB connection. DOAS intelligent system (DOASIS) software installed in the computer system was used for the operation of the instrument.

Figure 3. 1: Mini Max- DOAS

3.2. Monitoring sites and schedule

The Mini-MAX-DOAS was used for both fixed and mobile monitoring of HCHO. It was mounted on rooftop of IESE, NUST-Islamabad for regular fixed monitoring with elevation viewing angle settings of 2^0, 4^0, 5^0, 10^0, 15^0, 30^0, 45^0 and 90^0. Also, the instrument was used for mobile field campaigns in two mega cities of Pakistan (Lahore and Multan) and Stationary field campaigns in different forest types of Pakistan with elevation viewing angle settings of one 90^0 followed by four 30^0 angles. The reason for choosing angle of 90^0 was avoidance of interferences that might be caused by nearby substances while at the angle of 30^0 calculation of geometric Air Mass Factor (AMF) is easier.

Table 3.1: Schedule for continuous ground monitoring, and mobile and stationary field campaigns

Date	Study area	Area Category	Details of Activity
September 1,2015 – August 31,2018	IESE, NUST, Islamabad	Metropolitan city	Stationary continuous ground monitoring
July 12,2018	Shinkiari	Sub-Tropical Chir-Pine Forest	*FC-1: Stationary field campaign
July 13,2018	Shinkiari	Sub-Tropical Chir-Pine Forest	*FC-2: Stationary field campaign
July 14,2018	Shinkiari	National Tea Garden	*FC-3: Stationary field campaign
July 16,2018	Pine Park Hotel, Shogran	Moist Temperate Forest	*FC-4: Stationary field campaign
July 17,2018	Pine Park Hotel, Shogran	Moist Temperate Forest	*FC-5: Stationary field campaign
July 18,2018	Pine Park Hotel, Shogran	Moist Temperate Forest	*FC-6: Stationary field campaign
July 21,2018	Rama, Astore	Dry Temperate Forest	*FC-7: Stationary field campaign
July 22,2018	Deosai National Park	Alpine Pasture	*FC-8: Stationary field campaign

July 25,2018	Naran-Batakundi	Sub-Alpine Pasture	*FC-9: Stationary field campaign
October 26, 2018	Lahore	Metropolitan city	*FC-10: Mobile field campaign
October 27, 2018	Multan	Metropolitan city	*FC-11: Mobile field campaign
November 18, 2018	Multan	Metropolitan city	*FC-12: Mobile field campaign
November 19, 2018	Lahore	Metropolitan city	*FC-13: Mobile field campaign
December 15, 2018	Multan	Metropolitan city	*FC-14: Mobile field campaign
December 16, 2018	Lahore	Metropolitan city	*FC-15: Mobile field campaign
January 16, 2019	Lahore	Metropolitan city	*FC-16: Mobile field campaign
January 17, 2019	Multan	Metropolitan city	*FC-17: Mobile field campaign

*FC= Field Campaign

3.3. Algorithms and tools used in this research work

Formaldehyde was measured, analyzed and plotted by using several software listed in the table 3.2:

Table 3.2: List of Software used during the research work

Sr. #	Software	Purpose
1	DOASIS (Differential Optical Absorption Spectroscopy Intelligent System) (v 3.2.35)	Operating Software for MAX-DOAS and measurement of back scatter intensities
2	WinDOAS (Windows Differential Optical Absorption Spectroscopy)	Calibration process is performed.
3	QDOAS (v. 2.111.1)	Analysis of UV-Visible spectra to retrieve DSCDs
4	Microsoft Excel (v. 2016)	Mathematical Calculations for tropospheric VCD extraction and Graphical representations
5	ArcGIS (v. 10.3.1)	Interpolation of OMI Data and Validation of MAX-DOAS data with satellite observations

3.3.1. DOAS intelligent system (DOASIS)

The mini Max-DOAS was operated by DOASIS software to acquire data. The software is run by a java script with customized commands. The program adjusted the integration time of measured spectra, controlled the movement of the instrument by a stepper motor and regulated the temperature of the spectrometer. The ring spectrum was also calculated by this software.

In addition, the software was used for zero correction of the MAX-DOAS instrument. For this purpose, the dark current and offset were measured both automatically and manually

by using DOASIS at night time. Offset is the measurement of spectra by the spectrometer in dark. It was measured by setting 1000 number of scans and integration time of 100 milliseconds. Dark current on the other hand is the measure of small electric current passing through the spectrometer. It was measured by selecting number of scans to be 1 and integration time of 10000 milliseconds.

3.4. HCHO Analysis

The analysis of HCHO was carried out by the following these three steps:

i Wavelength Calibration

ii Convolution of reference spectra

iii DOAS fit analysis of HCHO

3.4.1. Wavelength Calibration

WinDOAS (Window differential optical absorption spectrometer) software was used for the purpose of wavelength calibration. The spectrum at 90^0 with highest concentration and least solar zenith angle at noontime (11:30 – 12:30) was selected for the calibration of wavelength. Retrieved spectrum was fitted to the convoluted solar spectrum in order to perform the calibration of the instrument. Solar spectrum wavelength was allocated to single detector's pixels for fitting process. The calibration fit attained is also labeled as "Kurucz-fit". The range of wavelength was further split into 6 sub-windows for performance and analysis of fits in respective sub-windows. In the process of calibration,

the shift of spectra amongst the measured and convoluted spectrum was adjusted by the function of “shift and squeeze”. For the interpolation of the results of each sub-window, the Slit function indicating the polynomial degree was utilized. By repeating the process of calibration for several times the residual error is minimized. The calibrated spectrum is used to calibrate the entire measured spectrums.

3.4.2. Convolution of reference spectra:

An important mathematical method, convolution, is used in wavelength processing operations. For performing convolution QDOAS software was used and the option of “Convolution tool” was selected in the software. Convolution has two types: 1) Online convolution 2) Offline convolution. In online convolution preprocessing of cross sections of various gases is not required because they get convoluted automatically during spectra analysis. In this type, cross-sections are simply put in formaldehyde analysis windows. While in case of offline convolution, convolution of cross-sections is required before putting them in formaldehyde analysis windows. In this study, online convolution method was used.

3.4.2.1. Convolution of cross-sections

The various trace gas cross-sections used in the process of convolution along with their specifications are enlisted in the table 3.3.

Table 3.3: Details of cross-sections used with convolution specifications

Sr. #	Cross Section	Convolution
1	hcho_297K_Meller	Standard Convolution
2	o4_thalman_volkamer_293K_inAir	Interpolate
3	bro_223K_Fleischmann	Standard Convolution
4	no2_298K_vanDaele	Convolve Io (1e17 molecule/cm^2)
5	o3_223K_SDY_air	Convolve Io (1e20 molecule/cm^2)
6	o3a_243p223K_SDY_336-359nm	Convolve Io (1e20 molecule/cm^2)
7	Ring (Ring_QDOAScalc_HighResSAO_Norm)	Ring Convolution

Gaussian shape was used as the slit function type with a FWHM of 0.7 nm. High resolution cross-sections were convoluted by using 'Standard convolution' option while for optical depth evaluation in the convolution, 'Convolve I0' option was selected (Fayt *et al.*, 2013).

3.4.3. Analysis of HCHO

QDOAS software was used for analysis purpose. In the display tab different fields (date, time, solar zenith angle and elevation viewing angle) are selected as shown in the figure.

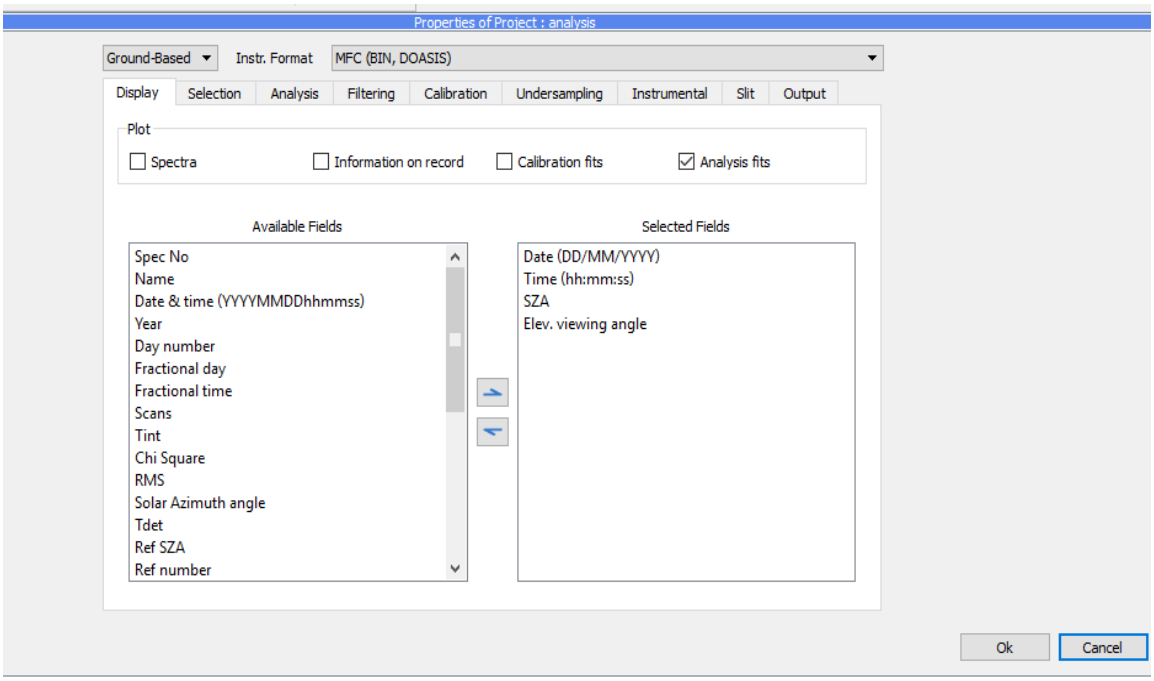

Figure 3. 2: Display tab on QDOAS software

Then in the instrumental tab offset, dark current and calibration file is selected and also the detector size of the instrument i.e. 2048 is entered manually.

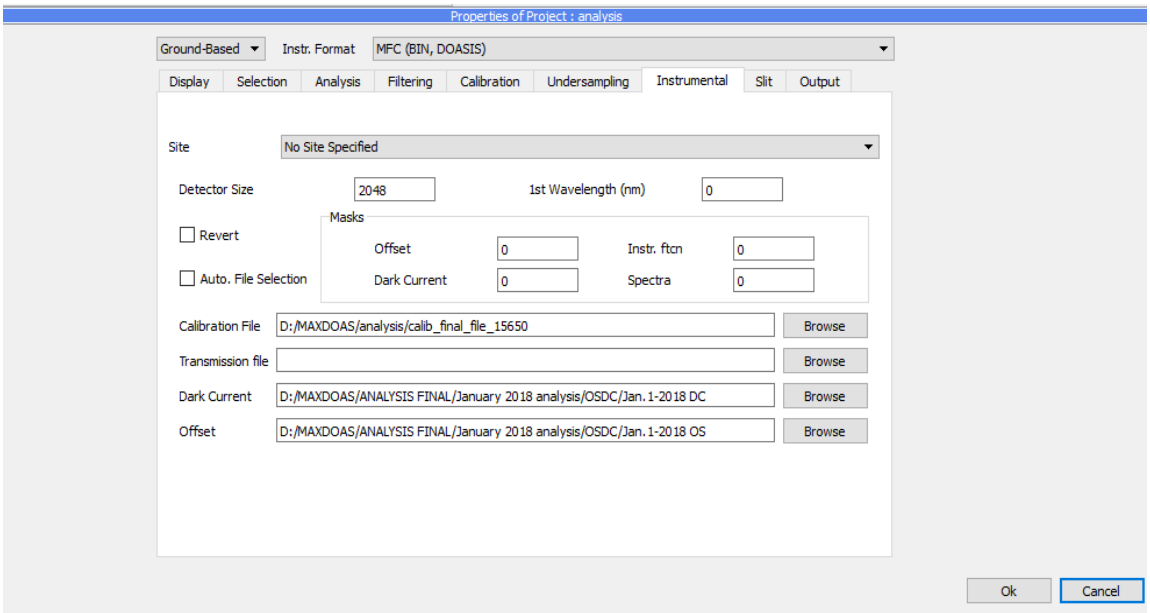

Figure 3. 3: Intrumental tab on QDOAS software

In the properties of analysis window for HCHO in QDOAS software, cross sections along with their suitable convolution settings were added in the molecules tab. And the fitting interval was set as 336.5-359nm. Also, the polynomial degree of order 5 was selected.

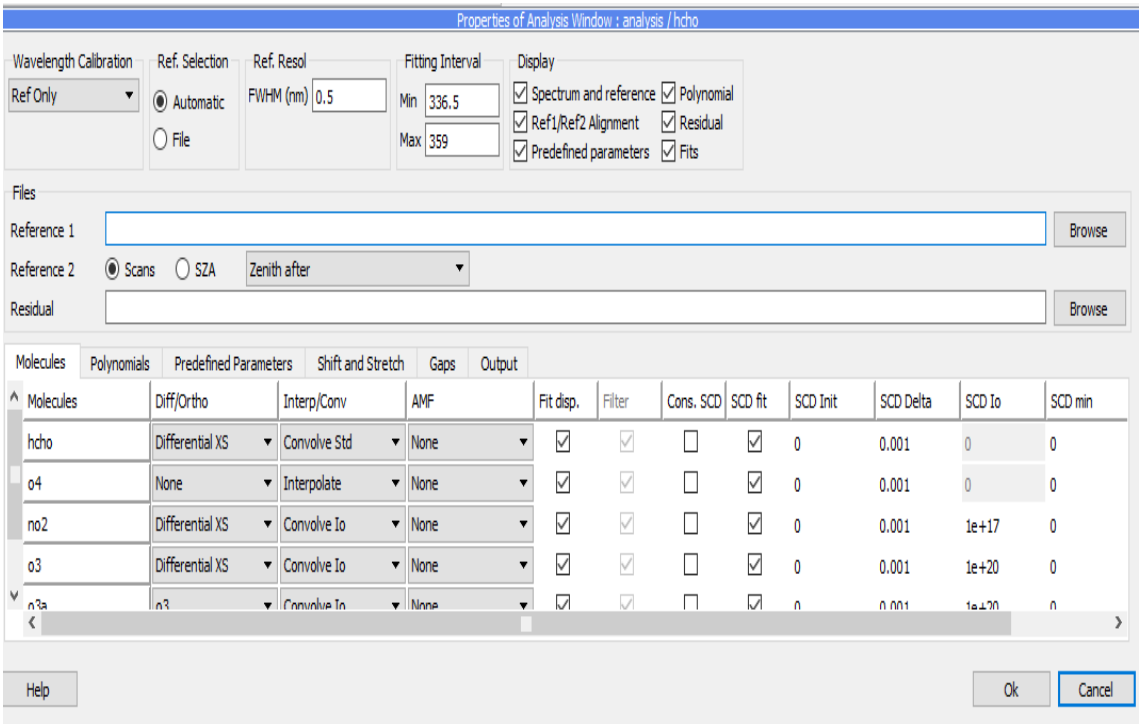

Figure 3. 4: Analysis window in QDOAS software

Then the output path was selected and finally analysis was run to obtain HCHO DSCDs in ascii file format. These files containing results of analysis are opened by using Microsoft Excel.

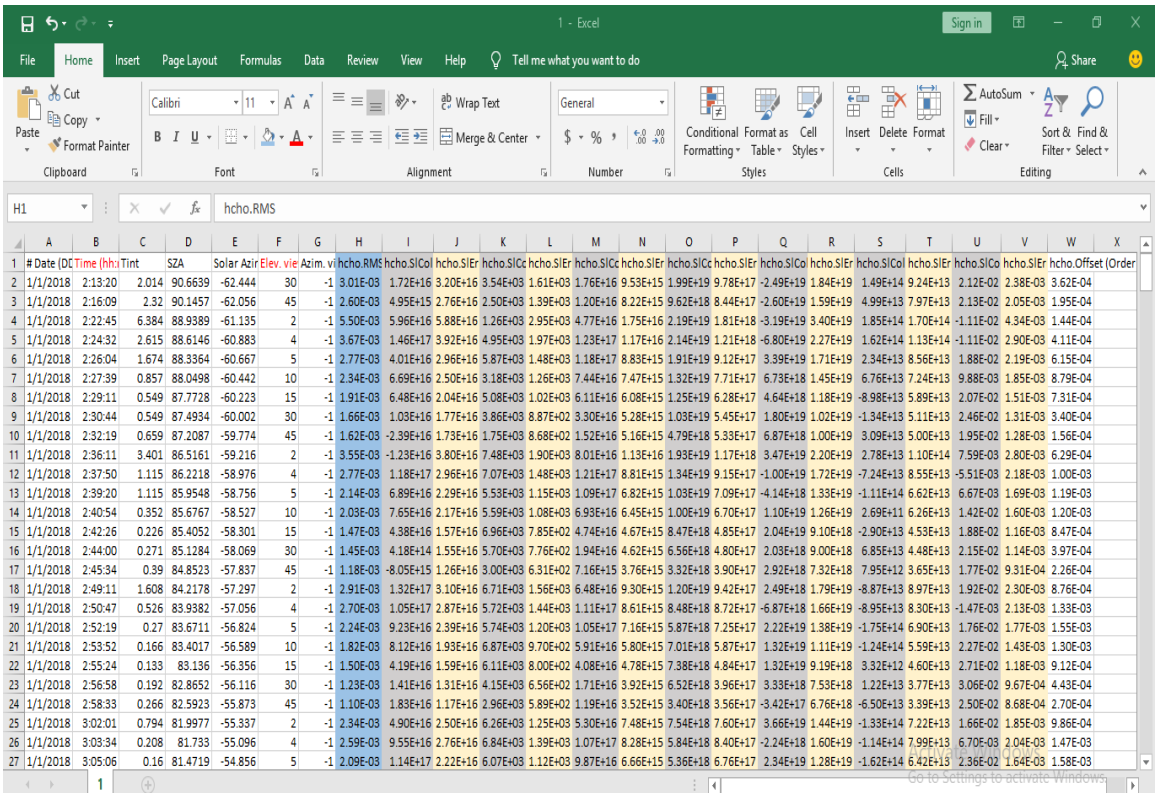

# Date (DD	Time (hh:i	Tint	SZA	Solar Azir	Elev. vie	Azim. vi	hcho.RMS	hcho.SlCol	hcho.SlEr	hcho.SlCo	hcho.SlEr	hcho.SlCo	hcho.SlEr	hcho.SlCo	hcho.SlEr	hcho.SlCo	hcho.SlEr	hcho.SlCol	hcho.SlEr	hcho.SlCo	hcho.SlEr	hcho.Offset (Order
1/1/2018	2:13:20	2.014	90.6639	-62.444	30	-1	3.01E-03	1.72E+16	3.20E+16	3.54E+03	1.61E+03	1.76E+16	9.53E+15	1.99E+19	9.78E+17	-2.49E+19	1.84E+19	1.49E+14	9.24E+13	2.12E-02	2.38E-03	3.62E-04
1/1/2018	2:16:09	2.32	90.1457	-62.056	45	-1	2.60E-03	4.95E+15	2.76E+16	2.50E+03	1.39E+03	1.20E+16	8.22E+15	9.62E+18	8.44E+17	-2.60E+19	1.59E+19	4.99E+13	7.97E+13	2.13E-02	2.05E-03	1.95E-04
1/1/2018	2:22:45	6.384	88.9389	-61.135	2	-1	5.50E-03	5.96E+16	5.88E+16	1.26E+03	2.95E+03	4.77E+16	1.75E+16	2.19E+19	1.81E+18	-3.19E+19	3.40E+19	1.85E+14	1.70E+14	-1.11E-02	4.34E-03	1.44E-04
1/1/2018	2:24:32	2.615	88.6146	-60.883	4	-1	3.67E-03	1.46E+17	3.92E+16	4.95E+03	1.97E+03	1.23E+17	1.17E+16	2.14E+19	1.21E+18	-6.80E+19	2.27E+19	1.62E+14	1.13E+14	-1.11E-02	2.90E-03	4.11E-04
1/1/2018	2:26:04	1.674	88.3364	-60.667	5	-1	2.77E-03	4.01E+16	2.96E+16	5.87E+03	1.48E+03	1.18E+17	8.83E+15	1.91E+19	9.12E+17	3.39E+19	1.71E+19	2.34E+13	8.56E+13	1.88E-02	2.19E-03	6.15E-04
1/1/2018	2:27:39	0.857	88.0498	-60.442	10	-1	2.34E-03	6.69E+16	2.50E+16	3.18E+03	1.26E+03	7.44E+16	7.47E+15	1.32E+19	7.71E+17	6.73E+18	1.45E+19	6.76E+13	7.24E+13	9.88E-03	1.85E-03	8.79E-04
1/1/2018	2:29:11	0.549	87.7728	-60.223	15	-1	1.91E-03	6.48E+16	2.04E+16	5.08E+03	1.02E+03	6.11E+16	6.08E+15	1.25E+19	6.28E+17	4.64E+18	1.18E+19	-8.98E+13	5.89E+13	2.07E-02	1.51E-03	7.31E-04
1/1/2018	2:30:44	0.549	87.4934	-60.002	30	-1	1.66E-03	1.03E+16	1.77E+16	3.86E+03	8.87E+02	3.30E+16	5.28E+15	1.03E+19	5.45E+17	1.80E+19	1.02E+19	-1.34E+13	5.11E+13	2.46E-02	1.31E-03	3.40E-04
1/1/2018	2:32:19	0.659	87.2087	-59.774	45	-1	1.62E-03	-2.39E+16	1.73E+16	1.75E+03	8.68E+02	1.52E+16	5.16E+15	4.79E+18	5.33E+17	6.87E+18	1.00E+19	3.09E+13	5.00E+13	1.95E-02	1.28E-03	1.56E-04
1/1/2018	2:36:11	3.401	86.5161	-59.216	2	-1	3.55E-03	-1.23E+16	3.80E+16	7.48E+03	1.90E+03	8.01E+16	1.13E+16	1.93E+19	1.17E+18	3.47E+19	2.20E+19	2.78E+13	1.10E+14	7.59E-03	2.80E-03	6.29E-04
1/1/2018	2:37:50	1.115	86.2218	-58.976	4	-1	2.77E-03	1.18E+17	2.96E+16	7.07E+03	1.48E+03	1.21E+17	8.81E+15	1.34E+19	9.15E+17	-1.00E+19	1.72E+19	-7.24E+13	8.55E+13	-5.51E-03	2.18E-03	1.00E-03
1/1/2018	2:39:20	1.115	85.9548	-58.756	5	-1	2.14E-03	6.89E+16	2.29E+16	5.53E+03	1.15E+03	1.09E+17	6.82E+15	1.03E+19	7.09E+17	-4.14E+18	1.33E+19	-1.11E+14	6.62E+13	6.67E-03	1.69E-03	1.19E-03
1/1/2018	2:40:54	0.352	85.6767	-58.527	10	-1	2.03E-03	7.65E+16	2.17E+16	5.59E+03	1.08E+03	6.93E+16	6.45E+15	1.00E+19	6.70E+17	1.10E+19	1.26E+19	2.69E+11	6.26E+13	1.42E-02	1.60E-03	1.20E-03
1/1/2018	2:42:26	0.226	85.4052	-58.301	15	-1	1.47E-03	4.38E+16	1.57E+16	6.96E+03	7.85E+02	4.74E+16	4.67E+15	8.47E+18	4.85E+17	2.04E+19	9.10E+18	-2.90E+13	4.53E+13	1.88E-02	1.16E-03	8.47E-04
1/1/2018	2:44:00	0.271	85.1284	-58.069	30	-1	1.45E-03	4.18E+14	1.55E+16	5.70E+03	7.76E+02	1.94E+16	4.62E+15	6.56E+18	4.80E+17	2.03E+18	9.00E+18	6.85E+13	4.48E+13	2.15E-02	1.14E-03	3.97E-04
1/1/2018	2:45:34	0.39	84.8523	-57.837	45	-1	1.18E-03	-8.05E+15	1.26E+16	3.00E+03	6.31E+02	7.16E+15	3.76E+15	3.32E+18	3.90E+17	2.92E+18	7.32E+18	7.95E+12	3.65E+13	1.77E-02	9.31E-04	2.26E-04
1/1/2018	2:49:11	1.608	84.2178	-57.297	2	-1	2.91E-03	1.32E+17	3.10E+16	6.71E+03	1.56E+03	6.48E+16	9.30E+15	1.20E+19	9.42E+17	2.49E+18	1.79E+19	-8.87E+13	8.97E+13	1.92E-02	2.30E-03	8.76E-04
1/1/2018	2:50:47	0.526	83.9382	-57.056	4	-1	2.70E-03	1.05E+17	2.87E+16	5.72E+03	1.44E+03	1.11E+17	8.61E+15	8.48E+18	8.72E+17	-6.87E+18	1.66E+19	-8.95E+13	8.30E+13	-1.47E-03	2.13E-03	1.33E-03
1/1/2018	2:52:19	0.27	83.6711	-56.824	5	-1	2.24E-03	9.23E+16	2.39E+16	5.74E+03	1.20E+03	1.05E+17	7.16E+15	5.87E+18	7.25E+17	2.22E+19	1.38E+19	-1.75E+14	6.90E+13	1.76E-02	1.77E-03	1.55E-03
1/1/2018	2:53:52	0.166	83.4017	-56.589	10	-1	1.82E-03	8.12E+16	1.93E+16	6.87E+03	9.70E+02	5.91E+16	5.80E+15	7.01E+18	5.87E+17	1.32E+19	1.11E+19	-1.24E+14	5.59E+13	2.27E-02	1.43E-03	1.30E-03
1/1/2018	2:55:24	0.133	83.136	-56.356	15	-1	1.50E-03	4.19E+16	1.59E+16	6.11E+03	8.00E+02	4.08E+16	4.78E+15	7.38E+18	4.84E+17	1.32E+19	9.19E+18	3.32E+12	4.60E+13	2.71E-02	1.18E-03	9.12E-04
1/1/2018	2:56:58	0.192	82.8652	-56.116	30	-1	1.23E-03	1.41E+16	1.31E+16	4.15E+03	6.56E+02	1.71E+16	3.92E+15	6.52E+18	3.96E+17	3.33E+18	7.53E+18	1.22E+13	3.77E+13	3.06E-02	9.67E-04	4.43E-04
1/1/2018	2:58:33	0.266	82.5923	-55.873	45	-1	1.10E-03	1.83E+16	1.17E+16	2.96E+03	5.89E+02	1.19E+16	3.52E+15	3.40E+18	3.56E+17	-3.42E+17	6.76E+18	-6.50E+13	3.39E+13	2.50E-02	8.68E-04	2.70E-04
1/1/2018	3:02:01	0.794	81.9977	-55.337	2	-1	2.34E-03	4.90E+16	2.50E+16	6.26E+03	1.25E+03	5.30E+16	7.48E+15	7.54E+18	7.60E+17	3.66E+19	1.44E+19	-1.33E+14	7.22E+13	1.66E-02	1.85E-03	9.86E-04
1/1/2018	3:03:34	0.208	81.733	-55.096	4	-1	2.59E-03	9.55E+16	2.76E+16	6.84E+03	1.39E+03	1.07E+17	8.28E+15	5.84E+18	8.40E+17	-2.24E+18	1.60E+19	-1.14E+14	7.99E+13	6.70E-03	2.04E-03	1.47E-03
1/1/2018	3:05:06	0.16	81.4719	-54.856	5	-1	2.09E-03	1.14E+17	2.22E+16	6.07E+03	1.12E+03	9.87E+16	6.66E+15	5.36E+18	6.76E+17	2.34E+19	1.28E+19	-1.62E+14	6.42E+13	2.36E-02	1.64E-03	1.58E-03

Figure 3. 5: Microsoft excel sheet showing results of HCHO analysis performed in QDOAS software

3.5. dAMF Calculation

Air mass factor was calculated by using Microsoft Excel. The ratio of direct incoming solar radiation path length to solar radiation path length coming vertically from the atmosphere is termed as air mass factor (AMF). While Differential AMF is the AMF difference between $\alpha \neq 90°$ and $\alpha = 90°$, while $\propto$ being the elevation angle. The off-axis view AMF can be evaluated as $1/\sin\alpha$ and zenith view AMF can be evaluated as 1 ($\sin 90° = 1$) respectively if the last scattering event of photons being recorded by the instrument happens to be higher than the layer of gas (Li et al., 2012).

$$\mathbf{dAMF(\alpha) = 1/\sin\alpha - 1} \qquad \mathbf{Eq.9}$$

3.6. Tropospheric VCD Calculation

The vertical column density (VCD) was calculated by converting AMF into dSCD. And from differential SCD, VCD was derived.

$$\mathbf{VCDgeo = dSCD\ (\alpha) / dAMF(\alpha)} \qquad \textbf{Eq. 10}$$

$$\mathbf{VCDgeo = dSCD\ (\alpha) / (1 / Sin\alpha)-1} \qquad \textbf{Eq. 11}$$

where α stands for elevation angle of the instrument. this specific method of calculating VCD is known as "geometric approach", therefore the VCD calculated are termed as VCDgeo.

3.7. Projection of Field Campaign VCDs

Maps were generated to present ground-based data monitored during the field campaigns along with satellite data for the respective days of the campaigns. ArcMap 10.3.1 was used to map the satellite data and ground based VCDs (as per the latitude and longitude measured using GPS).

3.8. Comparison of Ground based results with satellite data

The ground-based results were validated by comparing them with satellite data retrieved from OMI. Monthly Level 3 tropospheric satellite data was taken from TEMIS webpage (http://h2co.aeronomie.be/ch2o/ch2o.php?instr=omi&period=month) in ASCII format. Also OMI Level 2 total column data was downloaded from NASA's website (https://acdisc.gesdisc.eosdis.nasa.gov/opendap/HDFEOS5/Aura_OMI_Level2G/OMHCHOG.003/contents.html) in NetCDF 4 format.

Data downloaded in ASCII format was opened in ENVI +IDL 5.0 and tiff files were generated. The raster files in tiff format were opened in ArcMap 10.3.1. At first it was georeferenced and then spatial maps over the study area were generated using this software. The data files downloaded in NetCDF 4 format were opened in ArcMap 10.3.1 by making NetCDF raster layer file. The raster was then georeferenced and maps were generated.

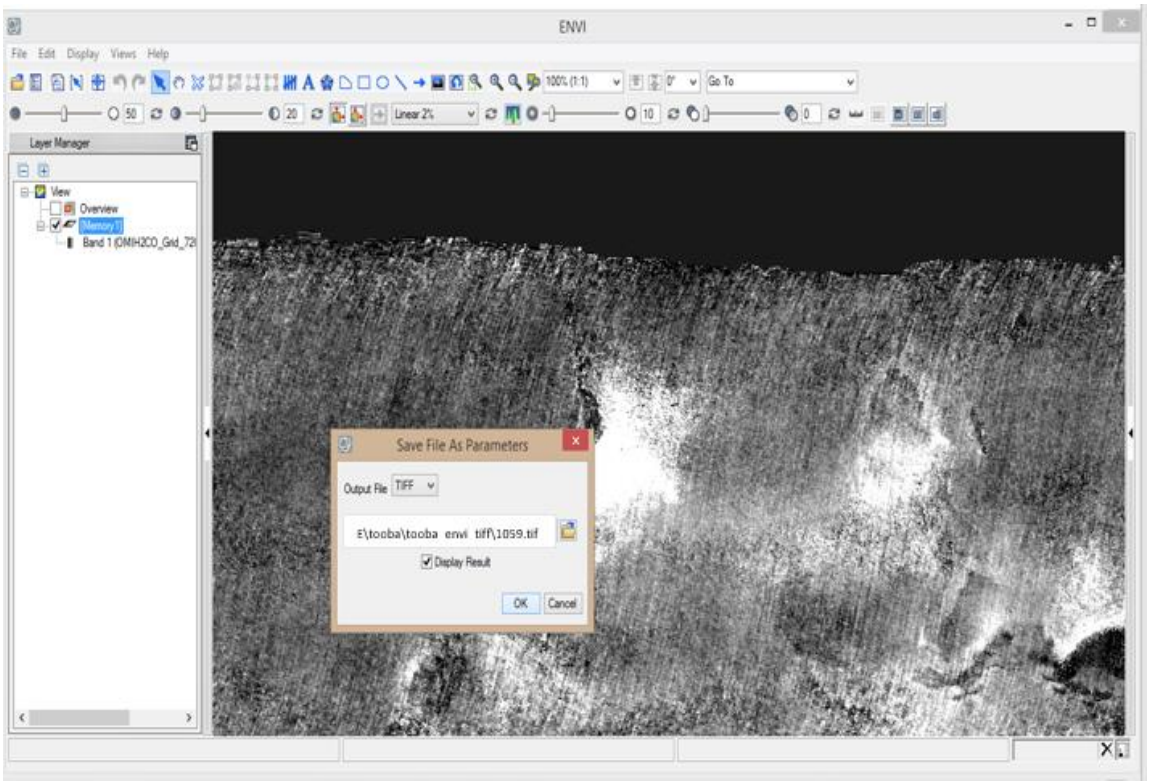

Figure 3. 6: Use of ENVI software for making TIFF file

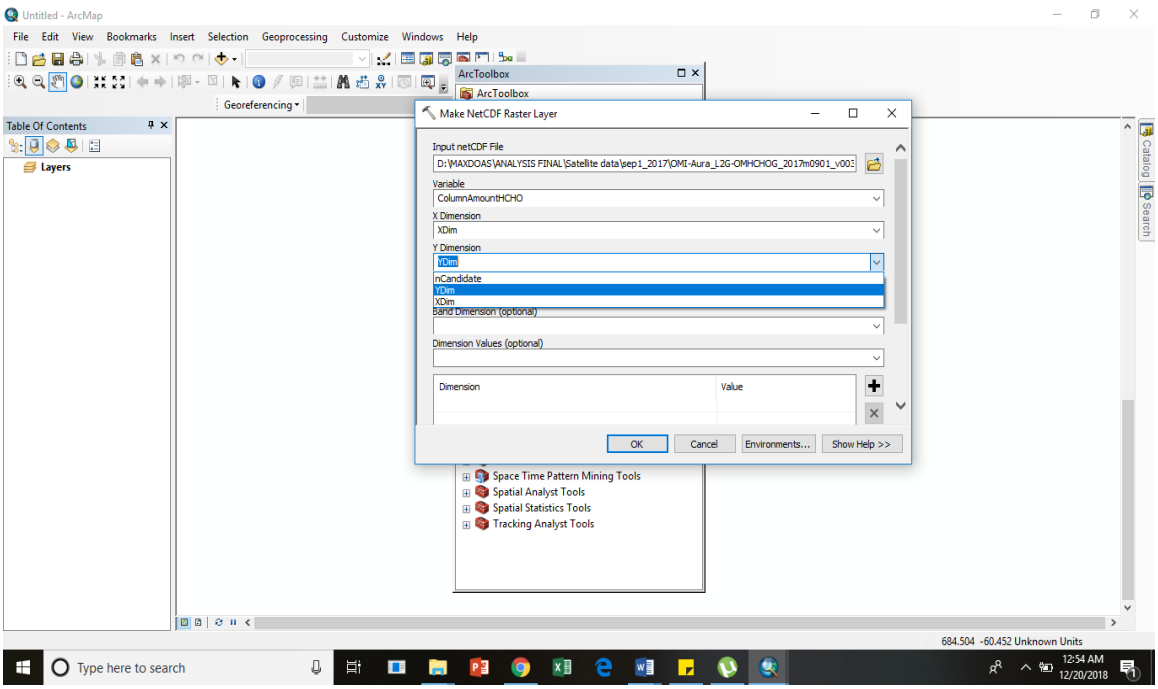

Figure 3. 7: ArcGIS 10.3 window showing making of NETCDF raster layer

The satellite data retrieved was then compared with ground-based data and results were generated.

4. Results and Discussion

4.1. HCHO Mixing Ratios Timeseries

Mixing ratio of HCHO were calculated by converting HCHO VCDs derived from MAX-DOAS ground-based monitoring to HCHO mixing ratios in parts per billion by volume (ppbv) considering that HCHO is concentrated near ground in the ambient air, close to its sources of emission. It was assumed that it lies between ground surface and 500 m above ground. It was observed that the average daily HCHO concentrations monitored during the study period were below the WHO threshold value of 83 ppbv.

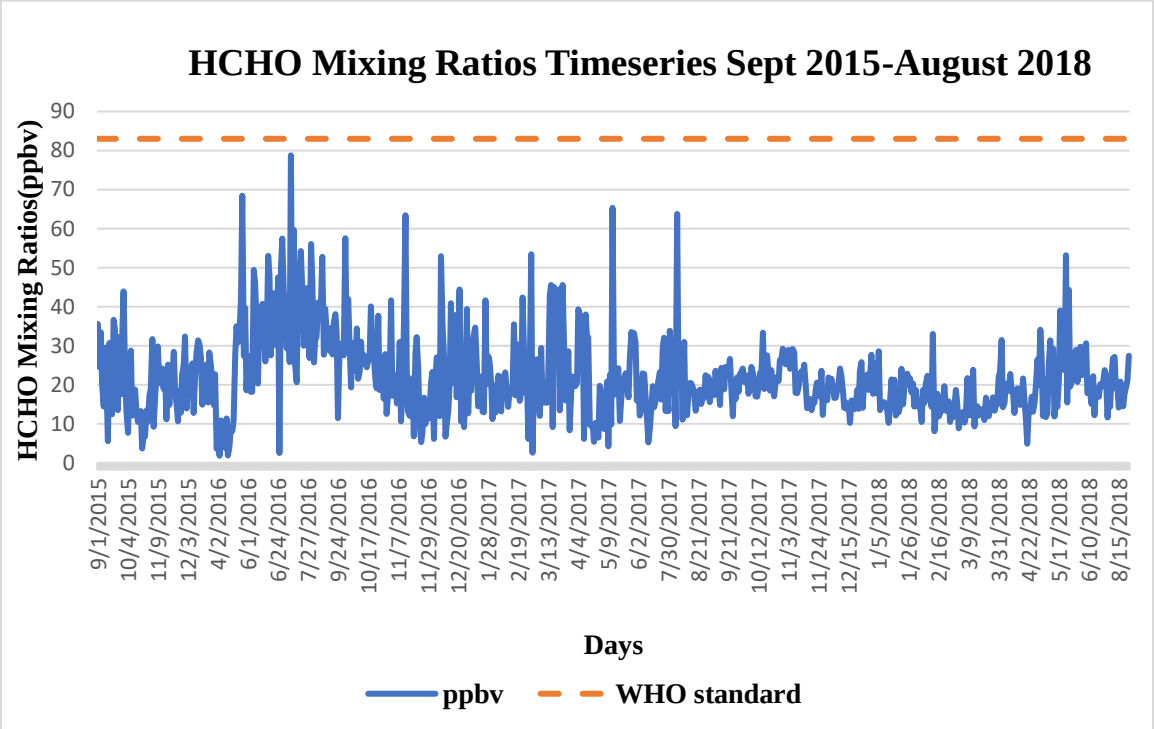

Figure 4. 1:HCHO daily average mixing ratios over IESE-NUST, Islamabad (dashed line is indicating WHO guideline for HCHO)

4.2. HCHO diurnal cycle over IESE-NUST

For the time period of September 2015 to August 2018 hourly average of the calculated VCDs over IESE, NUST was taken. These averages were used to derive the diurnal cycle of HCHO presented in Figure 4.2. In this graph, the annual HCHO diurnal cycle for 12 hours i.e. from 6 a.m. to 6 p.m. is shown because of instrument's limitation as it only operates in the presence of sunlight.

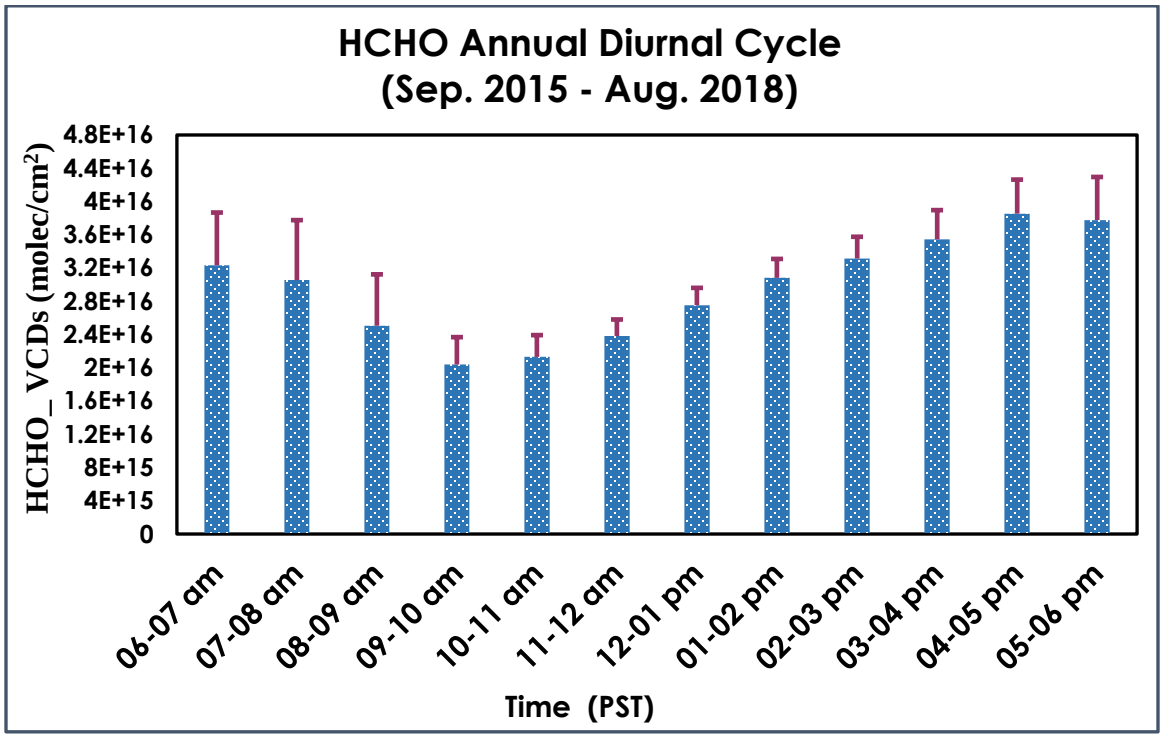

Figure 4. 2: Diurnal cycle (6am- 6pm) of average HCHO vertical column densities over IESE-NUST, Islamabad. Error bars are showing standard deviation for respective hour of the day.

HCHO concentration was found maximum during the early hours and at evening time. It is higher in the morning because of the background concentrations and lower solar intensity. As the solar intensity starts increasing the HCHO concentration starts to decline

reaching minima at 9-10 am due to photolysis and other chemical reactions. Till this time photolysis dominates over oxidation of methane and NMVOCs. However, from noon time and onward the HCHO concentrations starts increasing as the temperature increase which results in the increase of the biogenic emissions and thus the increase in the rate of VOC oxidation as well.

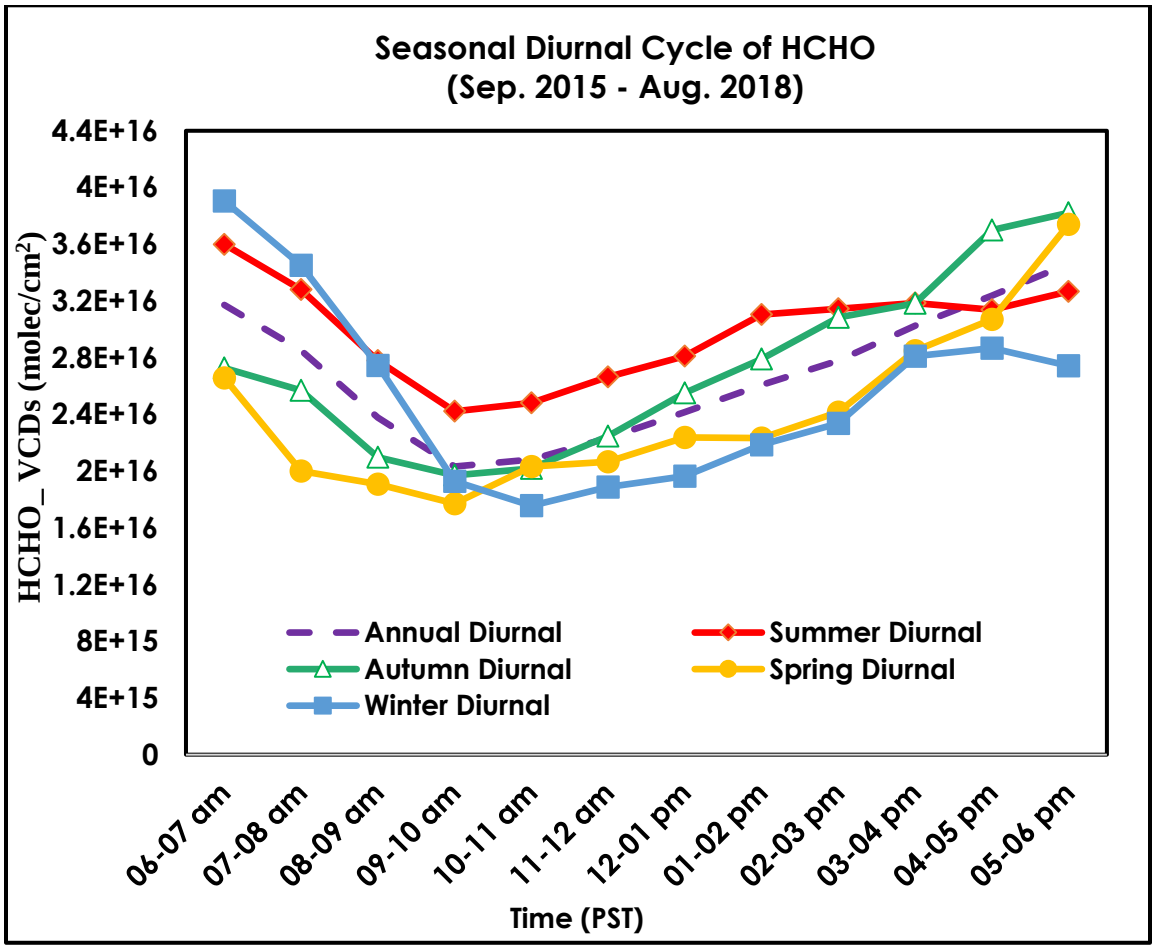

Figure 4. 3: Seasonal diurnal cycle (6am- 6pm) of average HCHO vertical column densities over IESE-NUST, Islamabad

Figure 4.3 shows the diurnal cycle of formaldehyde measured at IESE, NUST for different seasons. It can be observed that HCHO concentrations are found to be highest in summer

and lowest in winter (Gratsea et al., 2016) which is mainly due to the increased amount of biogenic emissions of NMVOCs (HCHO precursors) such as isoprene in summer as they are released into the atmosphere as a response of plants to heat stress (Siwko et al., 2007). While in winters plants are under minimum heat stress hence biogenic emissions are minimum. Also, HCHO values are higher during the early hours in winter. The reason for this could be the increased use of natural gas in offices and homes in the morning hours to cope up with cold weather, resulting in the increased level of methane in the atmosphere which upon oxidation forms HCHO as a byproduct. Moreover, in winters, solar intensity is low which results in slower photolysis and results in higher background HCHO concentrations are present in the atmosphere.

4.3. Weekly cycle of HCHO

The average weekly cycle shown in figure 4.4 depicts almost similar trend throughout the week. No weekend effect is observed mainly because Kashmir Highway adjacent to the study site is a busy road throughout the week. Also, HCHO concentrations in the ambient air are not solely due to the anthropogenic sources(transportation) but also because of the natural sources, in this case the vegetation cover in the surroundings of the study site.

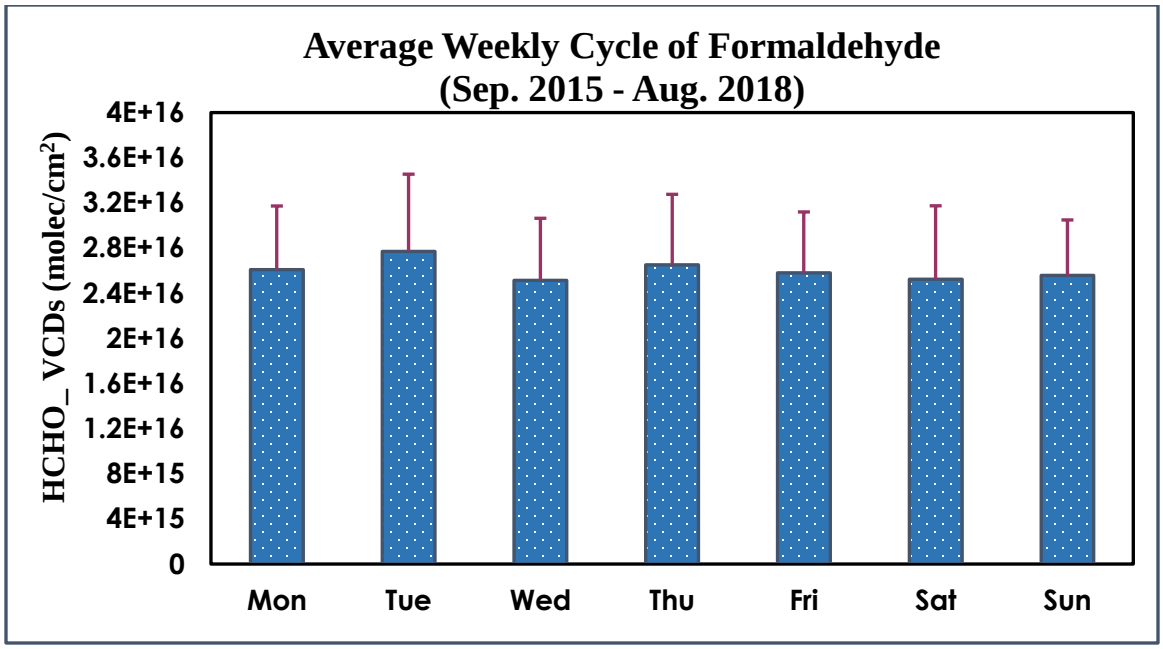

Figure 4. 4: HCHO weekly cycle over IESE-NUST monitored by using MAX-DOAS

4.4. Monthly cycle of HCHO

The average monthly cycle of HCHO from September 2015 to August 2018 is depicted in the figure 4.5. It is observed that the HCHO concentrations are comparatively lower in winters than in summers. This is due to the reason that in summer the biogenic emissions of NMVOCs, most prominently isoprene, increases as a result of plant response to heat stress. These precursors of HCHO gets oxidized in the atmosphere and produce HCHO as a byproduct. Furthermore, during summer, CH4 emission and oxidation caused by OH is maximum and results in higher amount of HCHO.

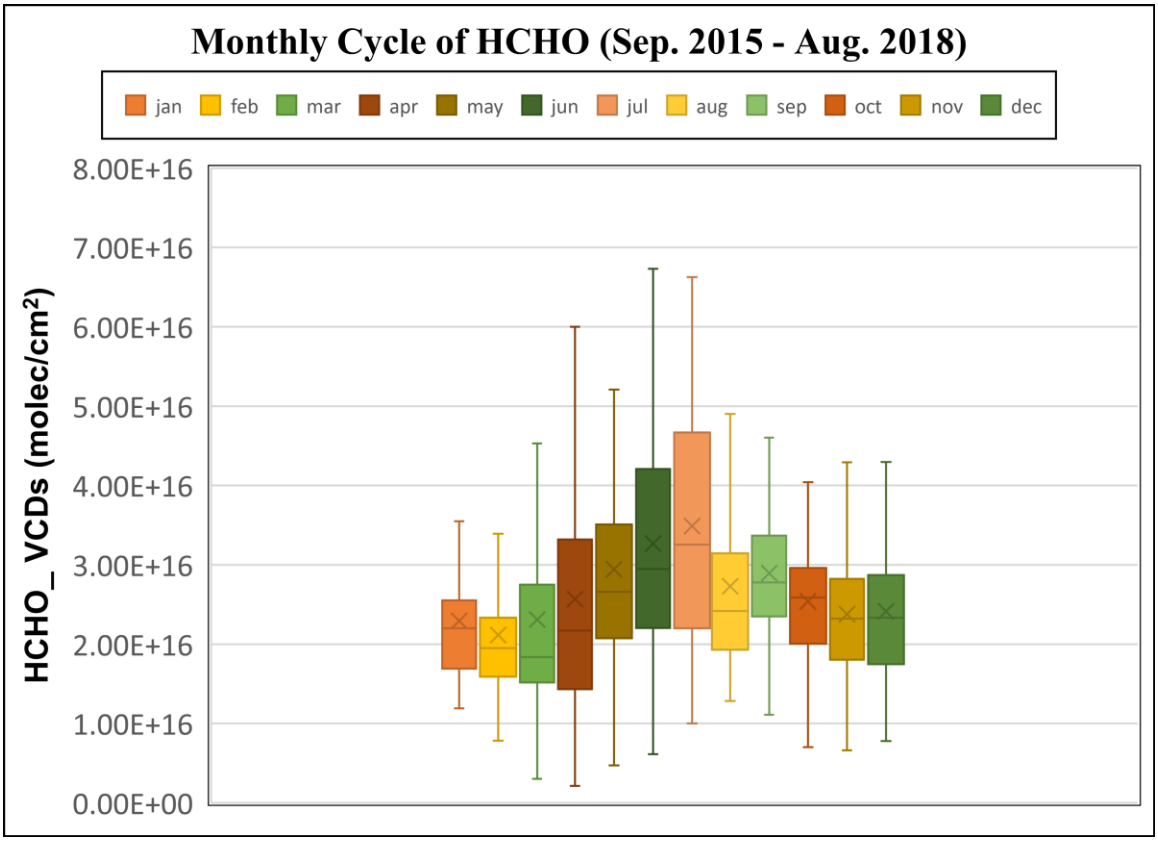

Figure 4. 5:HCHO monthly average VCDs over IESE-NUST observed using MAX-DOAS

4.5. Field campaigns

4.5.1. Forest field campaign

Vegetation is a prominent indirect source of HCHO in the atmosphere as it contributes majorly in the release of HCHO precursors (NMVOCs) such as isoprene into the atmosphere. For exploring this potential, MAX-DOAS instrument was taken to the forest areas in the north of Pakistan for HCHO monitoring. The average and maximum concentrations of HCHO were within the WHO threshold value of 83 ppbv. The maximum HCHO VCD i.e. 7.328E+16 was found on July 7,2018 in Sub-Tropical Chir-Pine Forest

located in Shinkiari, Pakistan. While on average the concentration of HCHO was highest in Tea Garden, Shinkiari. A study conducted by Menezes et al in 2019 revealed that the tea plant *Camellia sinensis* (grown in Tea Garden, Shinkiari) produce Volatile Organic Compounds (VOCs) such as terpenoids and terpenes (HCHO precursor) as secondary metabolites in leaves.

Table 4.1: Average and maximum HCHO concentration monitored during forest field campaigns

Study Site	***Date***	***Avg. HCHO VCD (molec/cm2)***	***Max. HCHO VCD (molec/cm2)***	***Max. HCHO VCD (ppbv)***
Shinkiari (Sub-Tropical Chir-Pine Forest)	7/12/2018	1.2611E+16	6.58E+16	56.02
Shinkiari (Sub-Tropical Chir-Pine Forest)	7/13/2018	1.1137E+16	7.328E+16	62.39
Tea Garden-Shinkiari	7/14/2018	1.9986E+16	6.676E+16	56.84
Shogran (Moist Temperate Forest)	7/16/2018	6.0005E+15	2.725E+16	23.20
Shogran (Moist Temperate Forest)	7/17/2018	6.8347E+15	2.501E+16	21.30
Shogran (Moist Temperate Forest)	7/18/2018	8.1018E+15	3.149E+16	26.81
Rama-Astore (Dry Temperate Forest)	7/21/2018	6.9621E+15	4.39E+16	37.38
Deosai (Alpine Pasture)	7/22/2018	6.8725E+15	2.17E+16	18.48
Naran-Batakundi (Sub-Alpine Pasture)	7/25/2018	9.0002E+15	3.879E+16	33.02

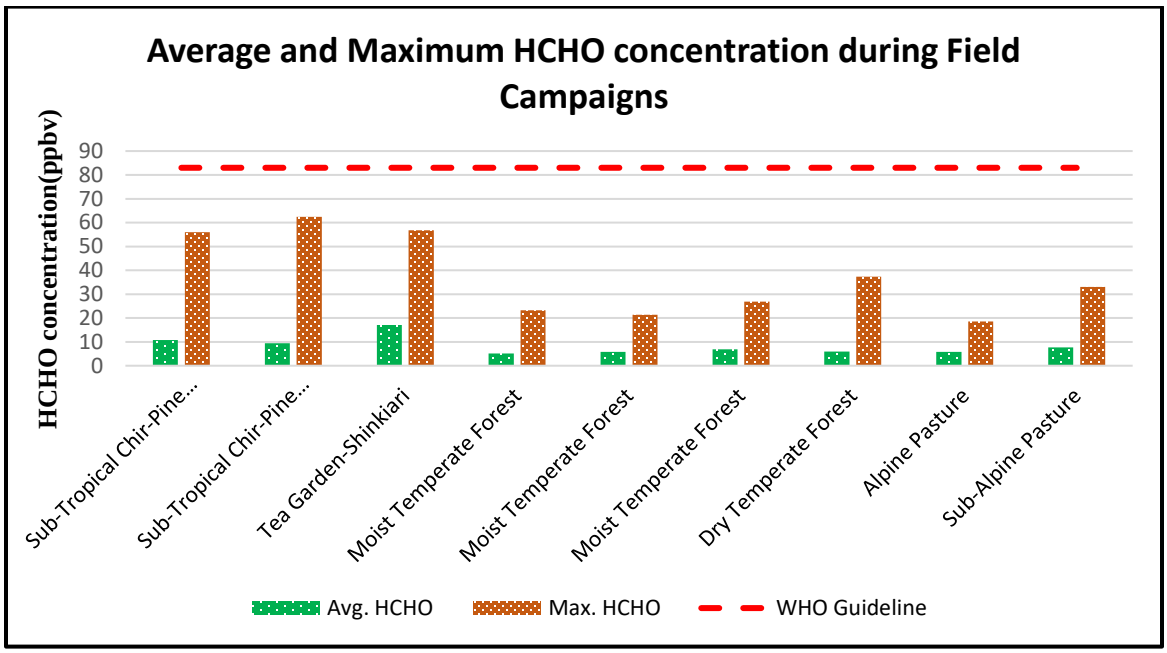

Figure 4. 6: Maximum and Average HCHO concentrations observed during Field Campaigns by using MAX-DOAS

4.5.2. Lahore and Multan field campaigns

Various field campaigns were conducted from October,2018 to January, 2019 in the city of Lahore and Multan in the time between sunrise to sunset.

Table 4.2: Average and maximum HCHO concentration monitored during Lahore and Multan field campaigns

Study Site	Date	Avg. HCHO VCD (molec/cm2)	Max. HCHO VCD (molec/cm2)	Max. HCHO Conc. (ppbv)
Lahore	26/10/2018	7.9705E+16	1.82532E+17	155.4169238
Multan	27/10/2018	1.90639E+16	3.33E+16	28.35329456

Multan (Round 1)	18/11/2018_R1	2.77083E+16	4.87E+16	41.46562898
Multan (Round 2)	18/11/2018_R2	2.19931E+16	3.55E+16	30.22648519
Lahore	19/11/2018	4.5256E+16	7.36E+16	62.66674112
Multan (Round 1)	15/12/2018_R1	2.93459E+16	4.6E+16	39.1667132
Multan (Round 2)	15/12/2018_R2	2.09446E+16	4.86046E+16	41.38440062
Lahore (Round 1)	16/12/2018_R1	3.406E+16	5.77E+16	49.12868156
Lahore (Round 2)	16/12/2018_R2	1.6456E+16	3.47E+16	29.54532496
Lahore (Round 1)	16/01/2019_R1	2.4758E+16	4.25E+16	36.1866372
Lahore (Round 2)	16/01/2019_R2	2.3418E+16	5.81357E+16	49.49965845
Multan (Round 1)	17/01/2019_R1	1.25436E+16	3.39E+16	28.86416473
Multan (Round 2)	17/01/2019_R2	8.05333E+16	3.18E+17	270.7611913

The route of the Lahore campaigns is shown in blue lines in the figure 4.7. The zones of traffic congestion along the route are depicted by red lines. Also, the major potential direct and indirect sources of HCHO in the Lahore city are shown in the figure 4.7.

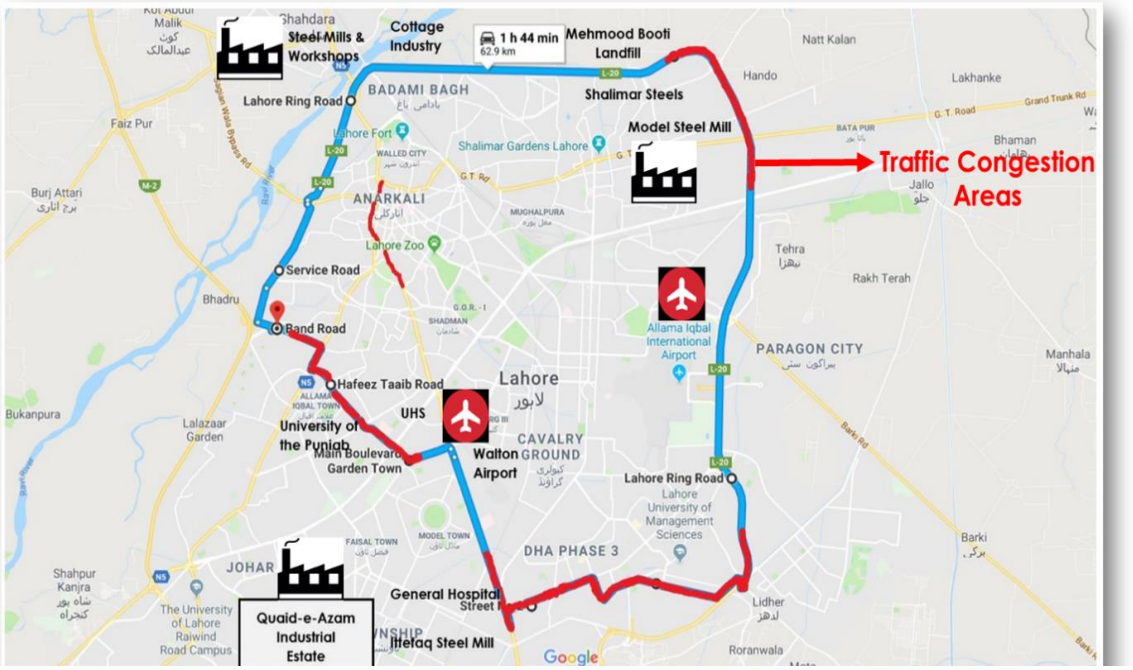

Figure 4. 7: Lahore field campaign route map for HCHO

The results for HCHO concentrations recorded along the ring road of Lahore, Pakistan by using car MAX-DOAS are depicted in Figure 4.7 along with the satellite data for the respective days of field campaigns retrieved from OMI. The legend of these maps representing the scale and color scheme for the HCHO concentrations along with the wind speed and wind direction (wind vector) is also shown in the figure. Map A, B and C in figure 4.8 depicts that the HCHO VCDs were high near traffic congestion areas, airport and Mehmood Booti landfill site. Map D shows that HCHO VCDs were high near steel mills, cottage industry and Mehmood Booti landfill site. While map E and F shows higher HCHO columns near steel mills, cottage industry, airport and traffic congestion areas. Overall, the VCDs of HCHO were found higher near Allama Iqbal International Airport, Mehmood Booti landfill site, industries and in areas of congested traffic.


26 OCT 2018 LAHORE
A


19 NOV 2018 LAHORE
B


16 DEC 2018 R1 LAHORE
C


16 DEC 2018 R2 LAHORE
D


16 JAN 2019 R1 LAHORE
E


16 JAN 2019 R2 LAHORE
F

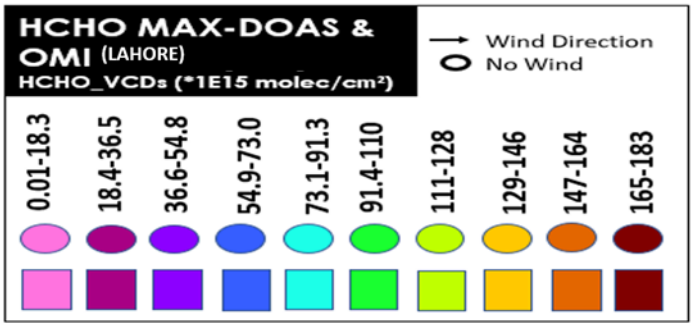

Figure 4. 8: HCHO VCDs retrieved from Car MAX-DOAS observations conducted in the city of Lahore along with satellite observations are depicted in map A, B, C, D, E & F. Wind vectors are also included in the maps in order to represent the average wind direction during particular field observations. Also, the legend for the maps is given.

The average and maximum concentrations of HCHO recorded in the Lahore city during the field campaigns are depicted in the figure 4.9. The maximum concentration on 26th October 2018 (155.4 ppbv) exceeded the WHO guideline (83 ppbv). On rest of the days the maximum and average concentrations were below the WHO threshold value.

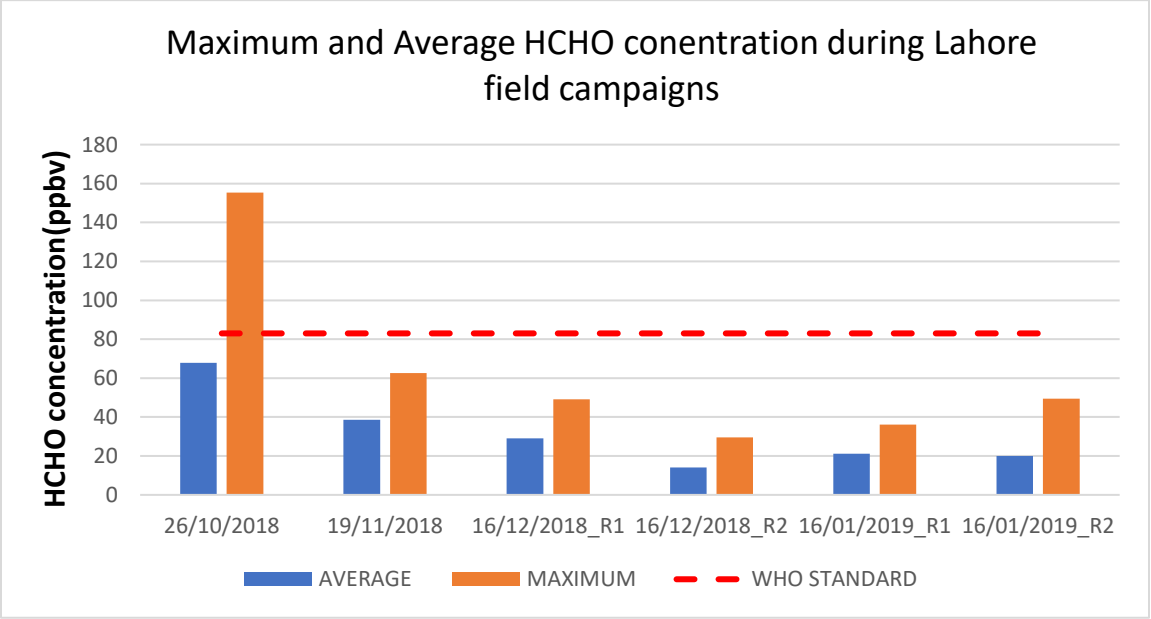

Figure 4. 9: ***Average and maximum HCHO concentration observed in Lahore City***

Field campaigns were also conducted in Multan, Pakistan by using CAR MAX DOAS. The route of the campaign is shown by blue lines figure 4.10. The traffic congestion areas along the route are depicted by orange lines. Also, the potential sources (direct and indirect) of HCHO in the city of Multan are mentioned in the figure below.

Figure 4. 10: Multan field campaign route map for HCHO

The results of both ground and satellite data for Multan field campaigns is shown in the maps in figure 4.11. Also, the legend of these maps representing the scale and color scheme for the HCHO columns along with the wind speed and wind direction (wind vector) is also shown. Map A, E and F shows that the values of HCHO VCDs were not much higher compared to other maps. Map B shows that HCHO columns were found to be higher near Fatima Fertilizers, airport and traffic congested areas. Map C shows that HCHO columns

were higher on N5 due to heavy traffic. Map D shows high HCHO columns near Fatima Fertilizers and on N5 due heavy traffic on this road. The HCHO concentrations were found higher in traffic congestion areas particularly in intercity areas of Multan. Also, higher HCHO concentrations were found near Fatima Fertilizer industry and other industrial units in Multan. However highest HCHO VCDs were found during round 2 on Jan 17, 2019 as shown in map G. This was mainly due to the longer traffic jam in the intercity area of Multan during that time of the campaign.

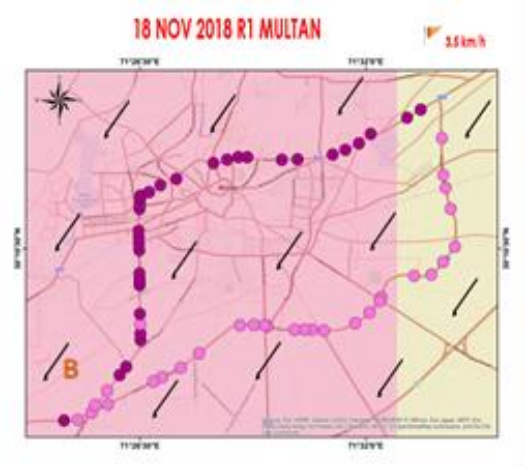

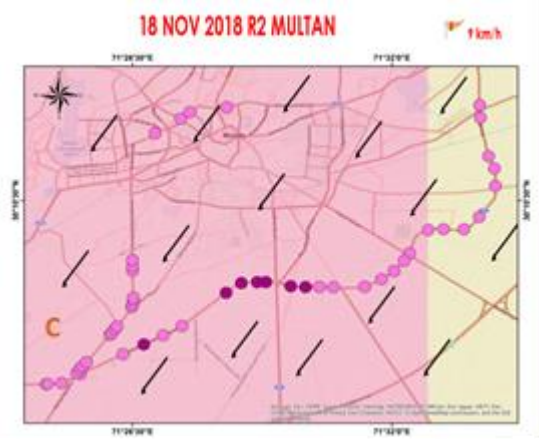

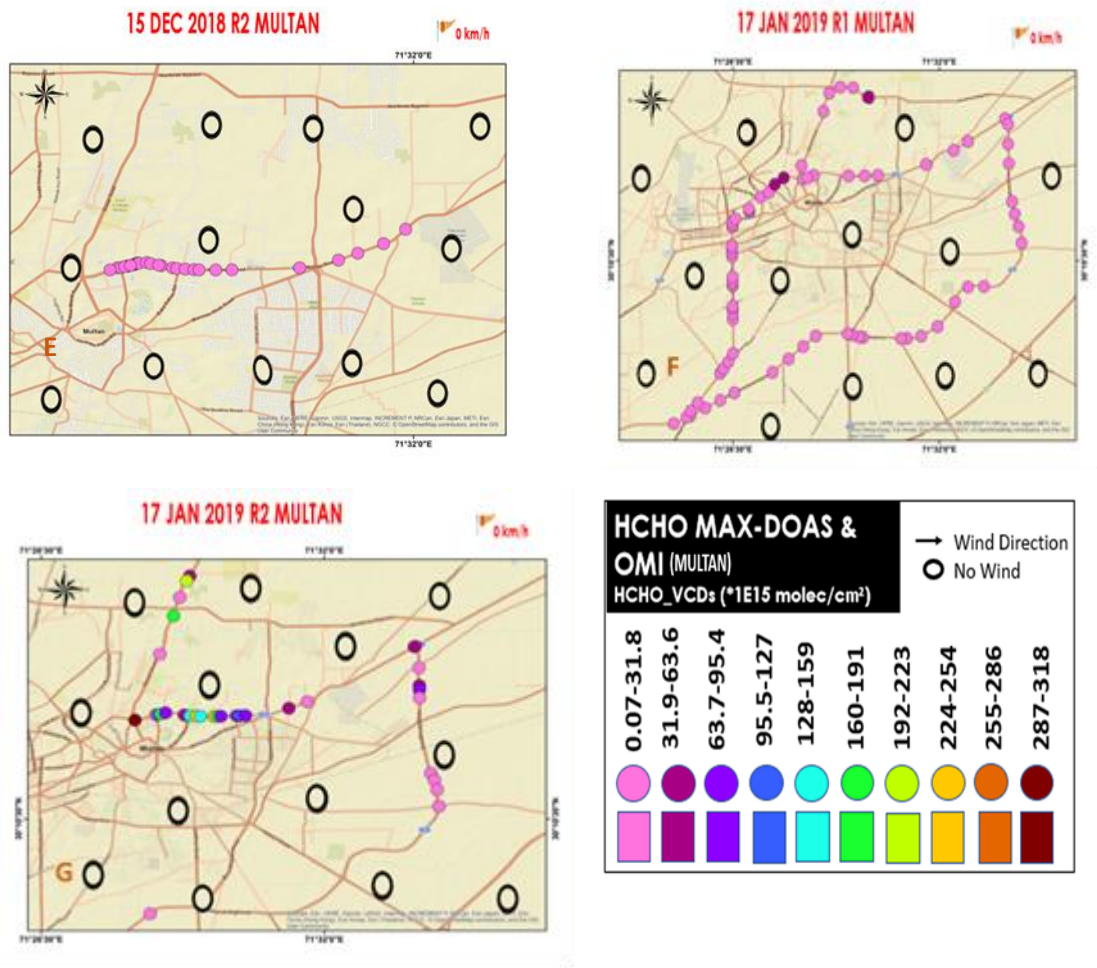

Figure 4. 11: HCHO concentrations retrieved from Car MAX-DOAS observations conducted in the city of Multan along with satellite observations are depicted in map A, B, C, D, E, F & G. Wind vectors are also included in the maps in order to represent the average wind direction during particular field observations.

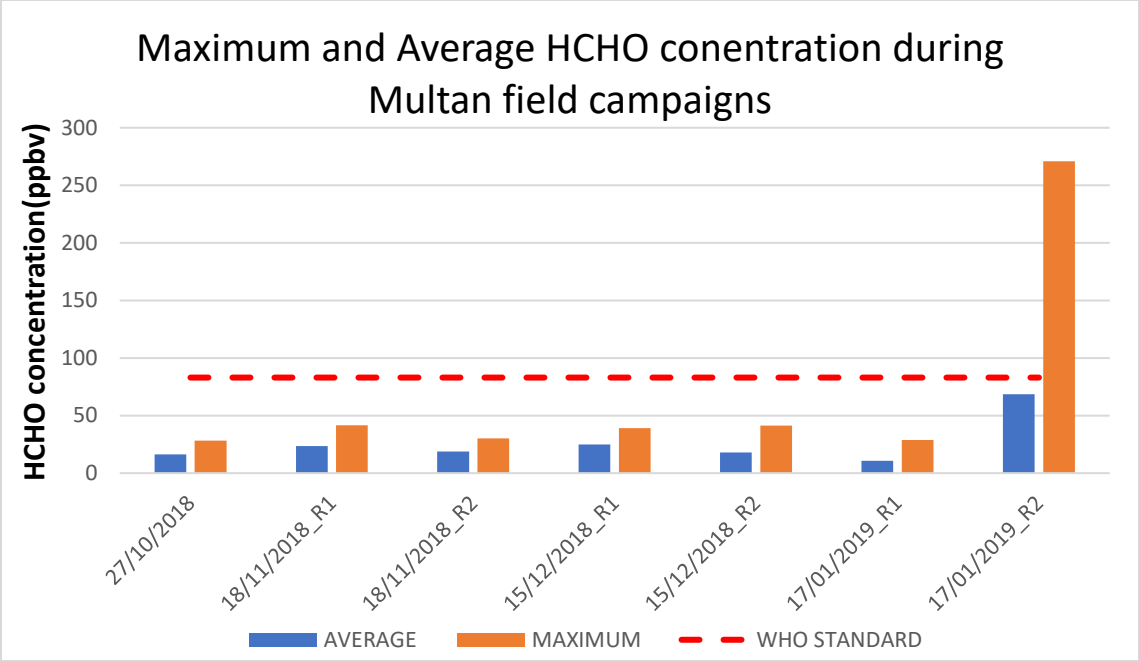

Figure 4. 12: Average and maximum HCHO concentration observed in Lahore City

4.6. Satellite validation of MAX-DOAS data

4.6.1. IESE-NUST site

The continuously monitored HCHO data at IESE-NUST by using MAX-DOAS was validated by comparing it with OMI data. The monthly average tropospheric HCHO data from OMI was only available from September 2015 till December 2016. While the onwards available data was daily average total column data from OMI till August 2018. Monthly mean was extracted from the daily data. The tropospheric and total column monthly data from OMI was compared with MAX-DOAS data for the respective months. The satellite data underestimated the ground-based HCHO MAX-DOAS observations. A

correlation with Pearson value of 0.68 and 0.59 was observed for comparison of both tropospheric and total column satellite data with ground-based results respectively.

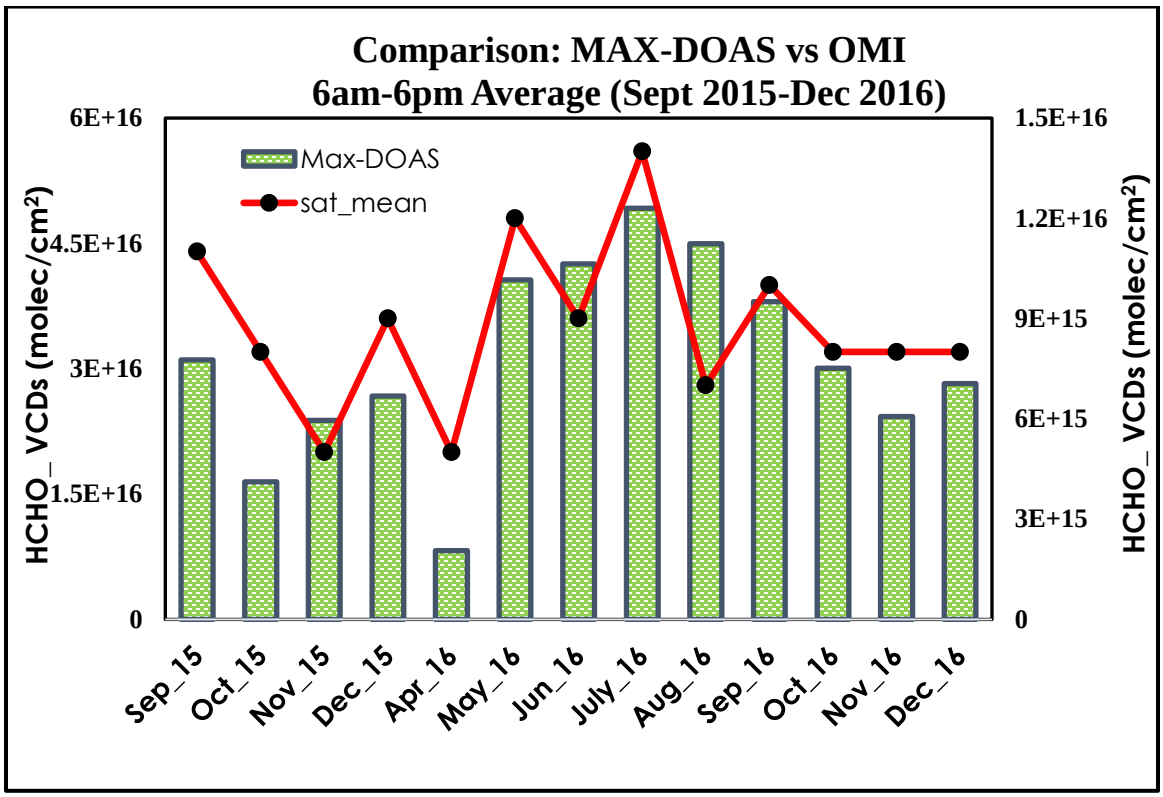

Figure 4. 13: HCHO monthly average of MAX-DOAS (6am to 6pm) vs OMI tropospheric HCHO monthly average over IESE-NUST, Islamabad

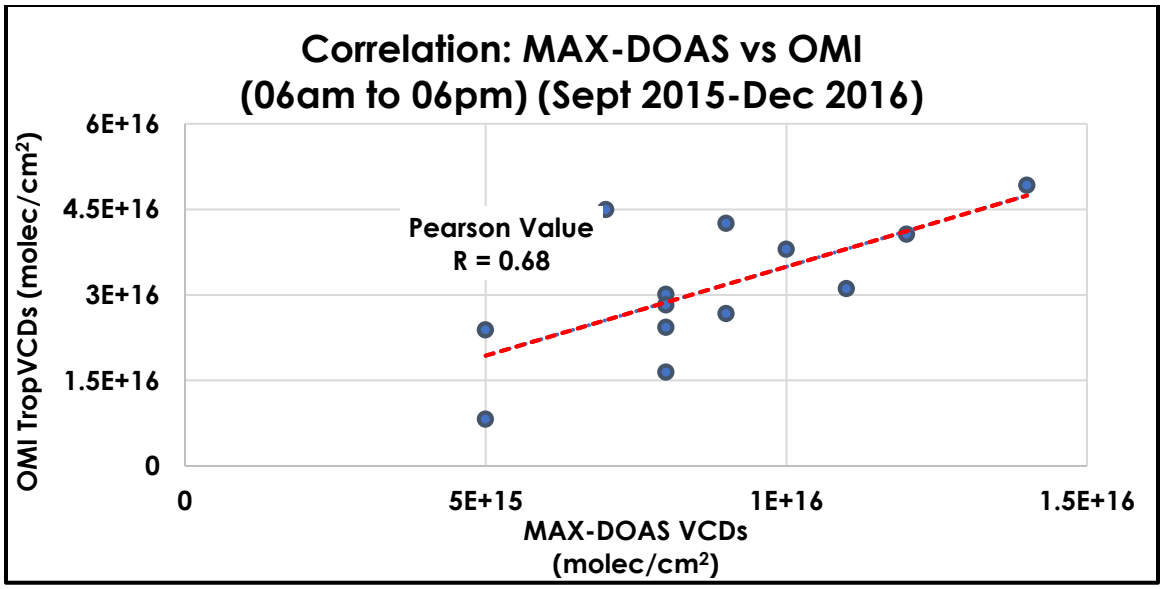

Figure 4. 14: Correlation between HCHO monthly average of MAX-DOAS (6am to 6pm) vs OMI tropospheric HCHO monthly average over IESE-NUST, Islamabad

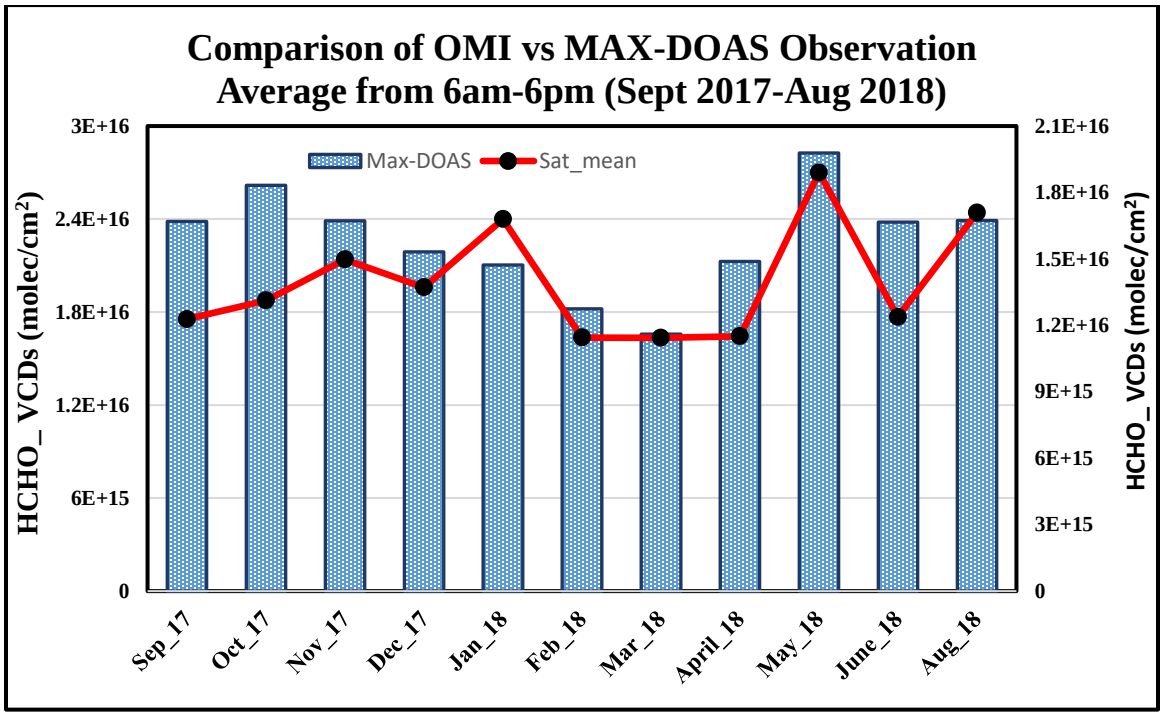

Figure 4. 15: HCHO monthly average of MAX-DOAS (6am to 6pm) vs OMI total column HCHO monthly average over IESE-NUST, Islamabad

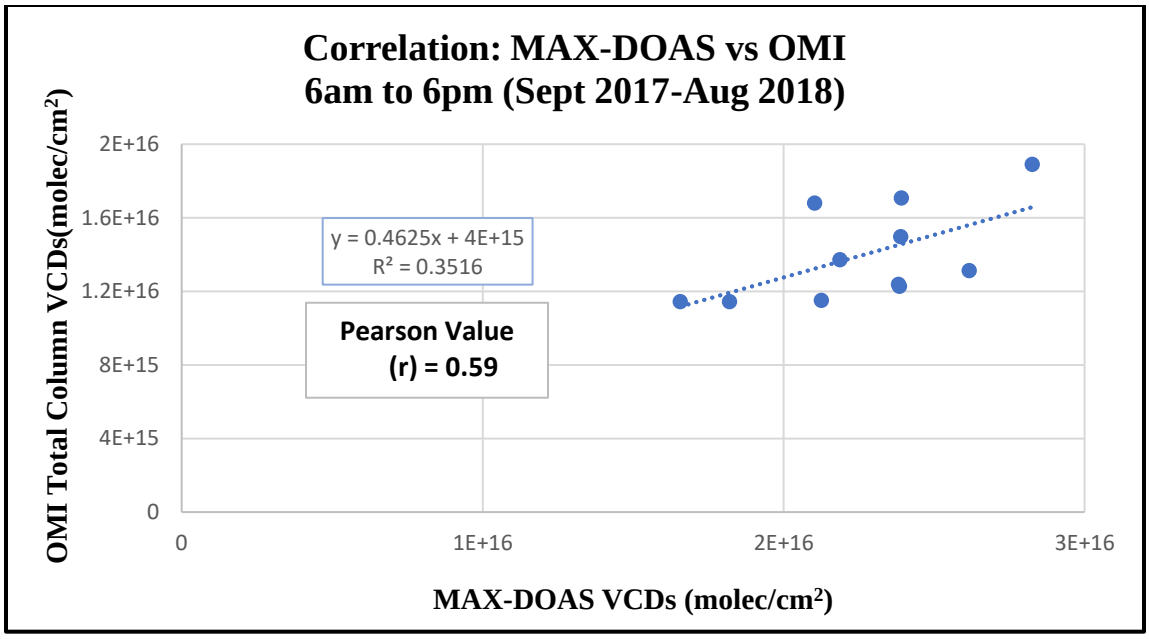

Figure 4. 16: Correlation of HCHO monthly average of MAX-DOAS (6am to 6pm) vs OMI total column HCHO monthly average over IESE-NUST, Islamabad

4.6.2. Forest field campaigns

The total column OMI satellite data for the respective days of forest field campaigns downloaded from GISDISC website was compared with the ground based VCDs (calculated by using MAXDOAS) of respective forest campaign days by mapping both datasets on ArcMap (figure 4.17).

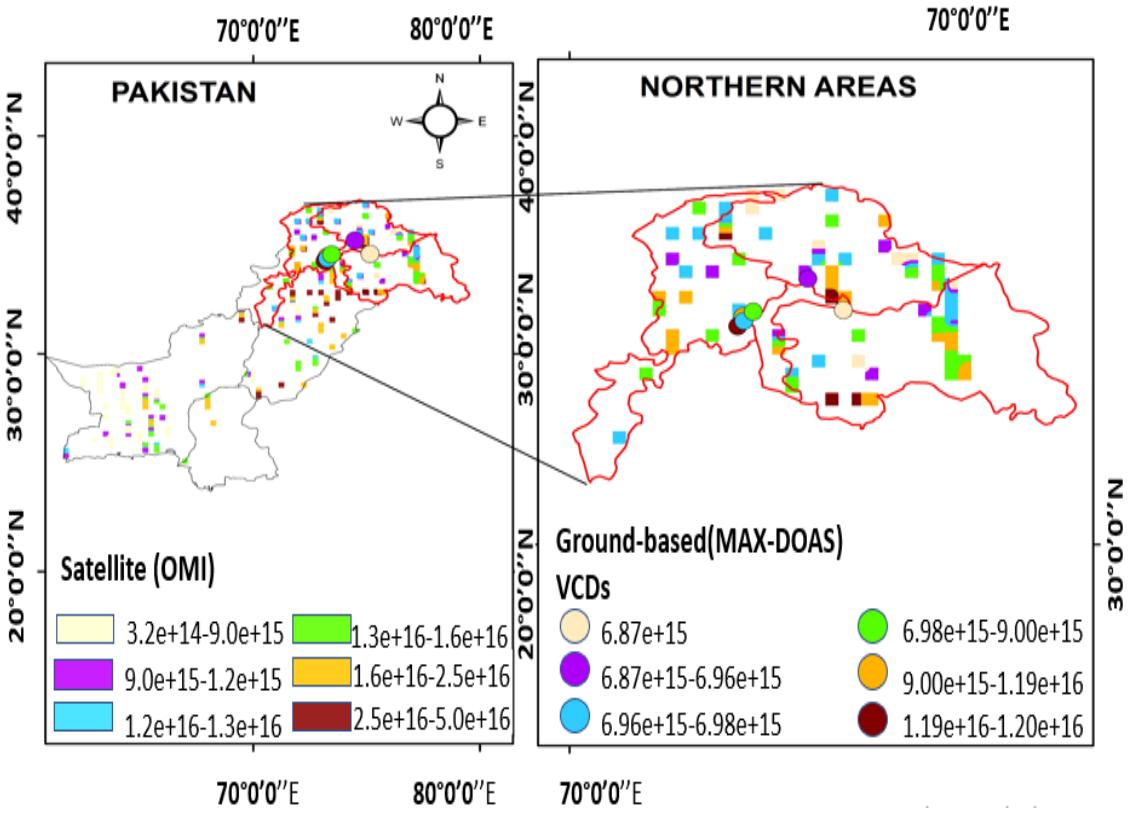

Figure 4. 17: Forest campaign ground-based data vs satellite data

4.7. Industrial Natural Gas-An anthropogenic source of HCHO

Methane oxidation in the atmosphere leads to the formation of formaldehyde. It is one of the major anthropogenic sources of HCHO. In this study, the natural gas used in industries located in Islamabad were compared with the ground based HCHO concentrations recorded over Islamabad. The data of industrial natural gas was collected from Sui Northern Gas Pipelines Limited. The comparison showed that the concentration of HCHO in the atmosphere does vary with the use of natural gas (figure 4.18). A correlation of 0.60 was

observed for the monthly natural gas used by the industries and HCHO concentrations measured (4.19).

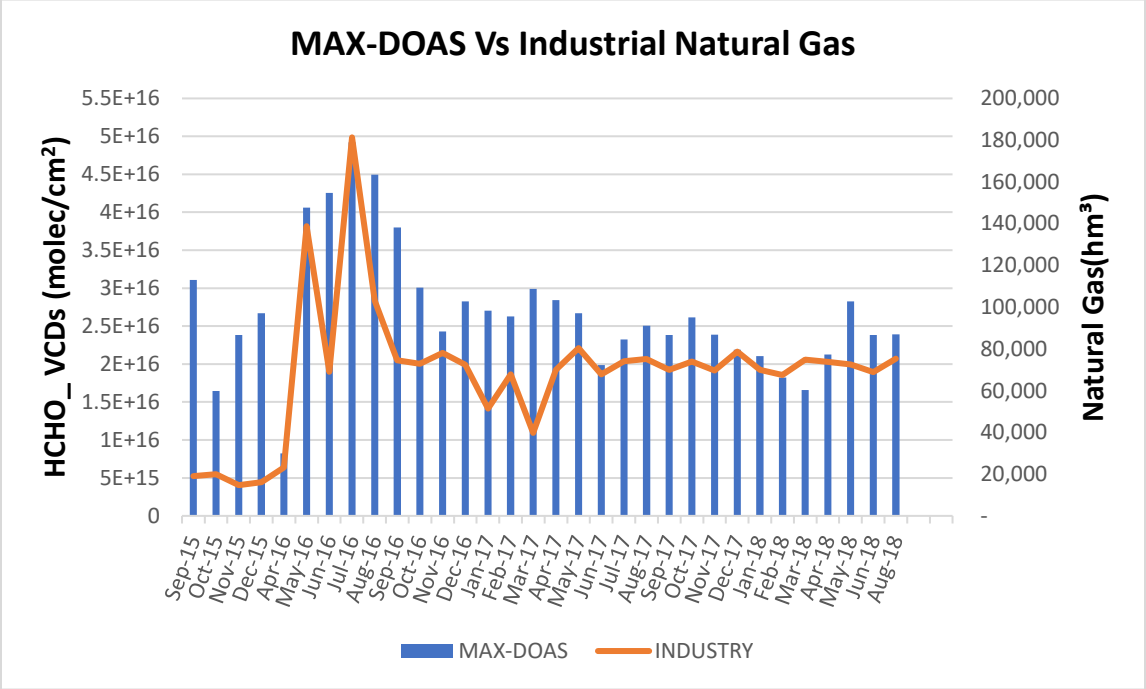

Figure 4. 18: Monthly average HCHO VCDs observed vs Natural Gas Used in Islamabad

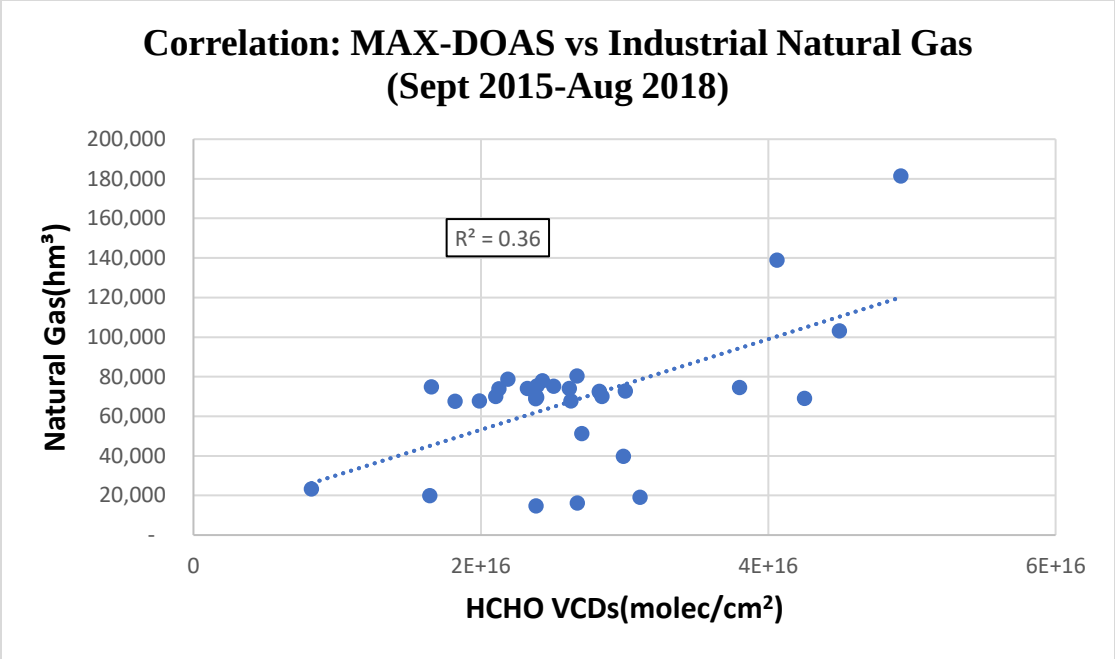

Figure 4. 19: Comparison of Monthly average HCHO VCDs observed vs Natural Gas used in Islamabad

4.8. Vegetation- A natural source of HCHO emissions

4.8.1. IESE-NUST site

The HCHO VCDs were compared with NDVI data for IESE-NUST site (Figure 4.20) as vegetation is major source HCHO precursors, NMVOCs such as isoprene. A positive correlation showing pearson value of 0.53 was observed (Figure 4.21). However, the satellite NDVI data underestimates the actual ground vegetation cover in summers due deficiency of chlorophyll caused by heat stress in summer months.

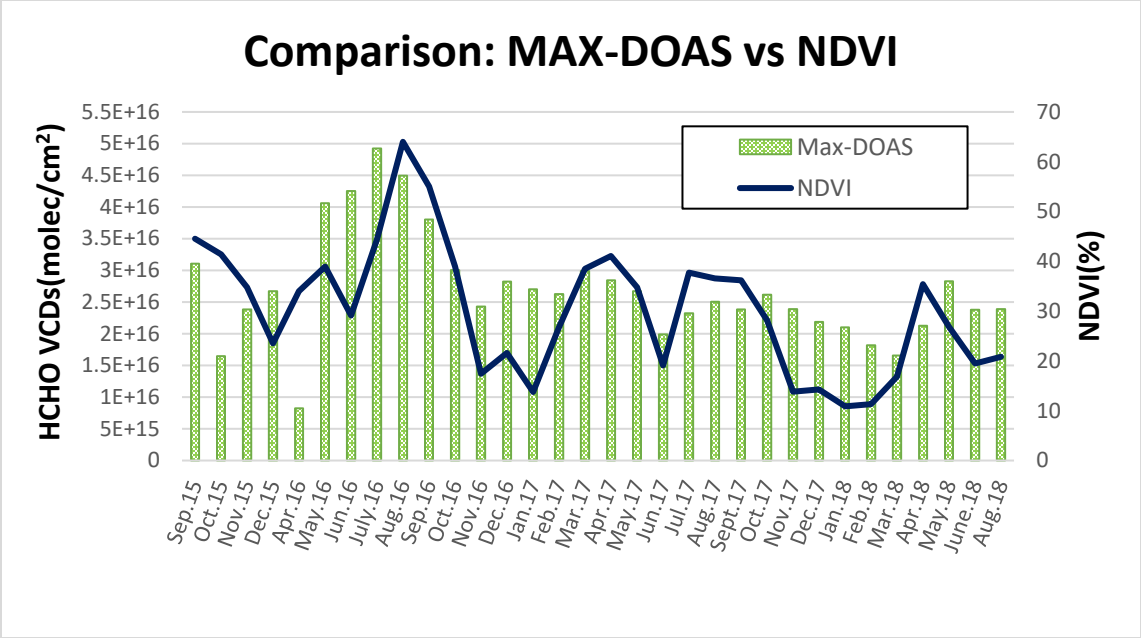

Figure 4. 20: Comparison of MAX-DOAS monthly average VCDs of HCHO vs NDVI over IESE-NUST, Islamabad

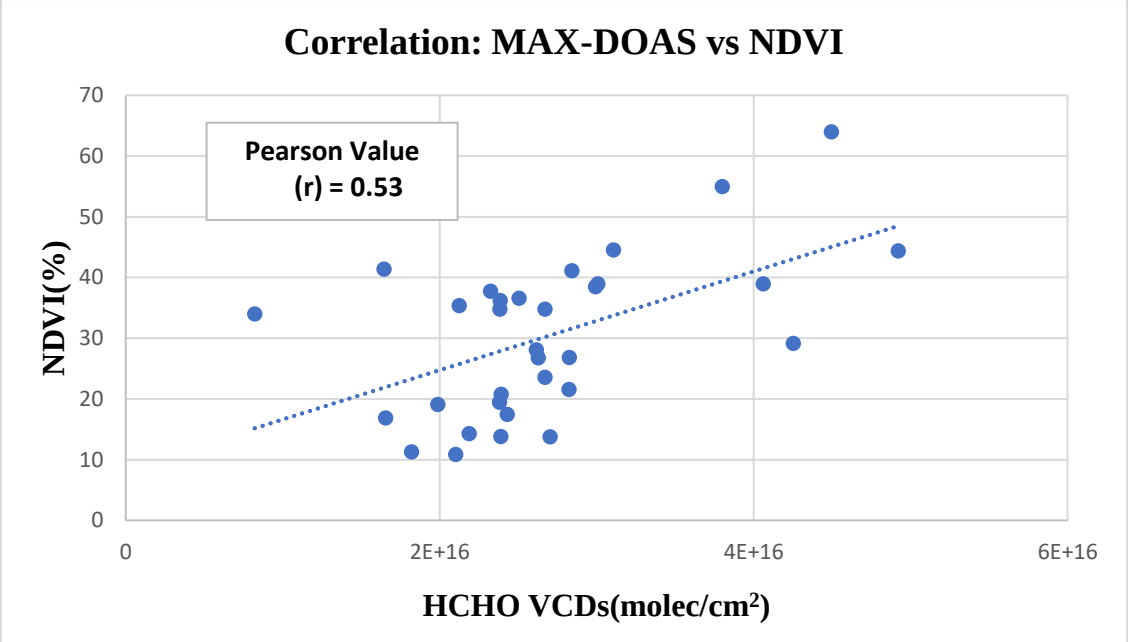

Figure 4. 21: Correlation of MAX-DOAS monthly average VCDs of HCHO vs NDVI over IESE-NUST, Islamabad

4.9. Temperature dependence of HCHO Concentrations

Plants release NMVOCs under heat stress, which are the precursors of HCHO in the atmosphere and contributes majorly in HCHO formation in the atmosphere. To validate this point temperature data was compared with ground-based MAX-DOAS VCDs observed during the study period (Figure 4.22). Temperature showed a strong correlation with MAX-DOAS measurements over Islamabad (Pearson value r = 0.86) as depicted in Figure 4.23.

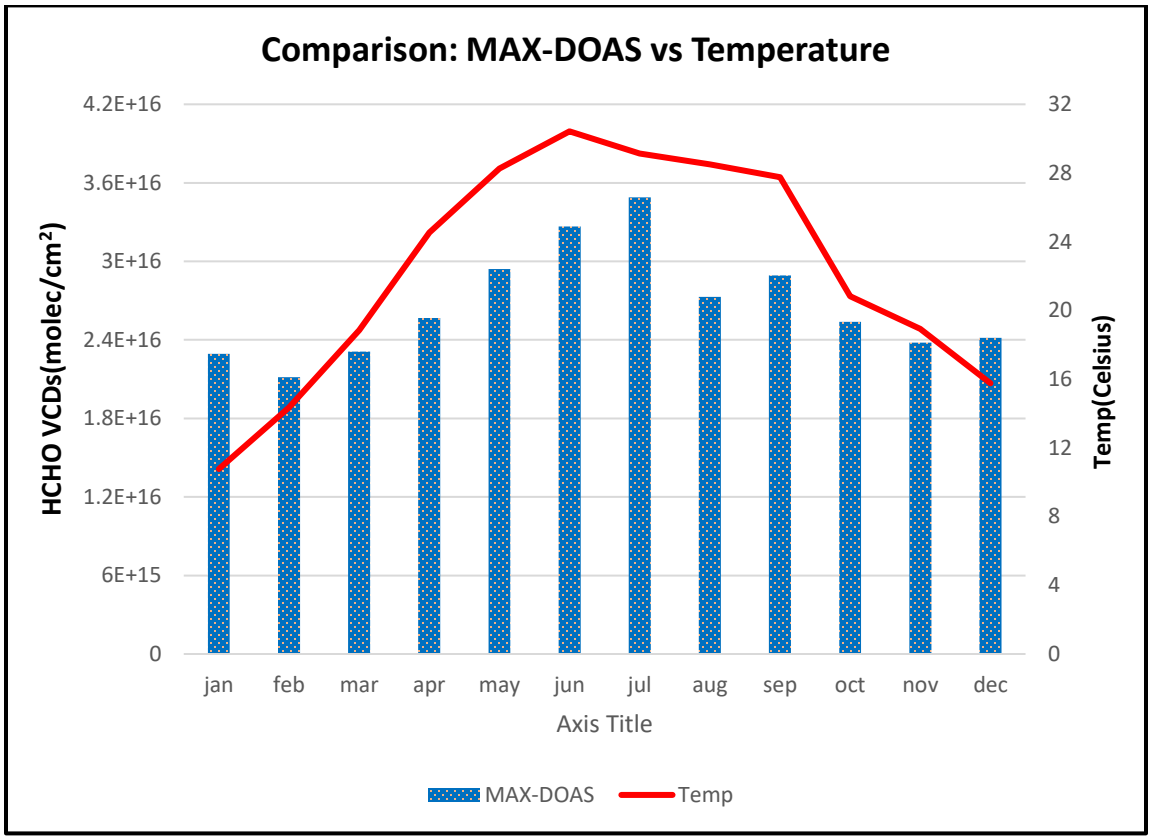

Figure 4. 22: Comparison of MAX-DOAS monthly average VCDs vs monthly average Temperature over Islamabad

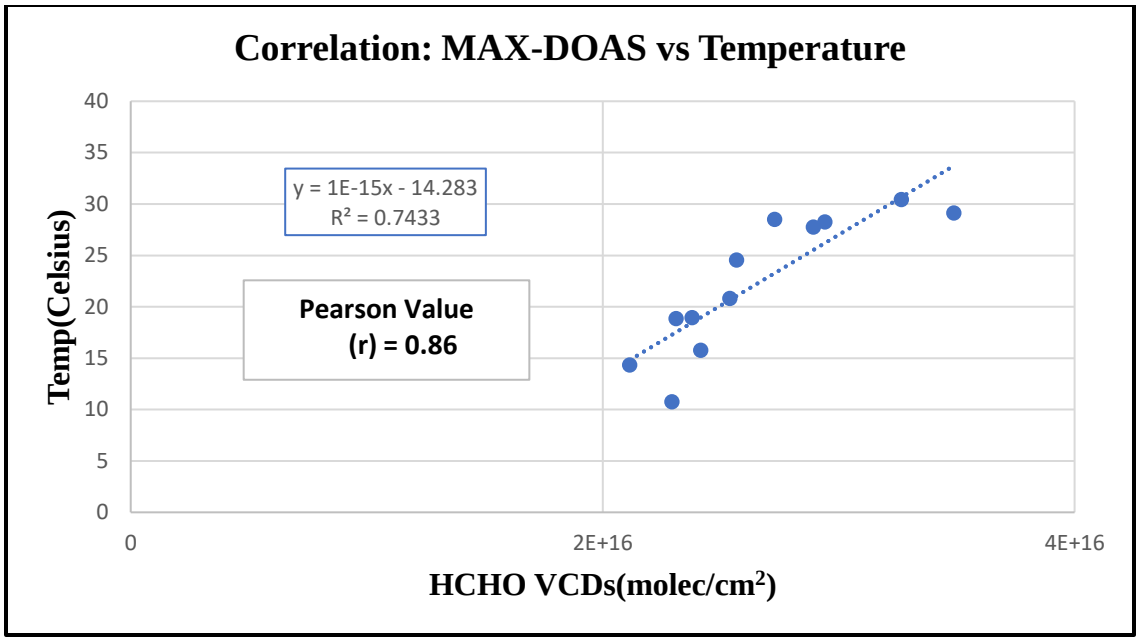

Figure 4. 23: Correlation of MAX-DOAS monthly average HCHO VCDs vs monthly average Temperature over Islamabad

VCDs measured by using MAX-DOAS during the field campaigns carried out in the different forest types of Pakistan were also compared with the daily average temperature for the respective locations (figure 4.24). Comparison of temperature with MAX-DOAS data for the field campaigns (figure 4.25) also showed a good correlation (Pearson value r = 0.71) further validating the point that temperature increase results in the increase of HCHO in the atmosphere in areas having vegetation in its vicinity.

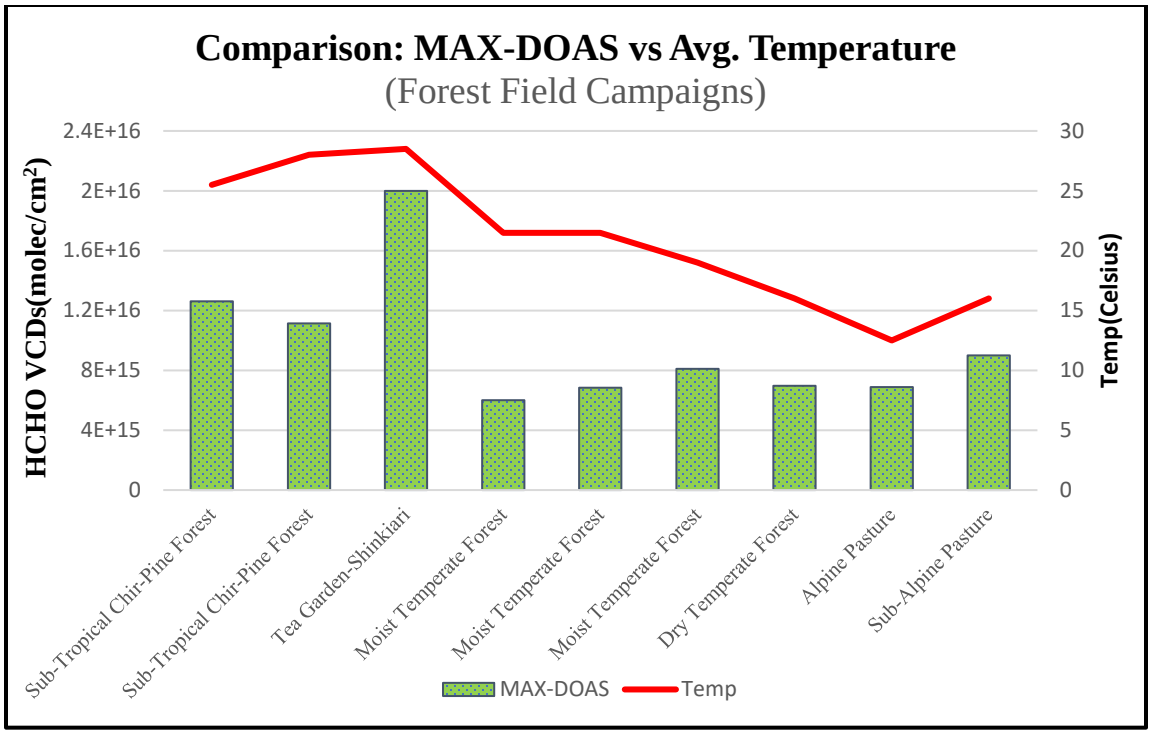

Figure 4. 24: Comparison of MAX-DOAS average HCHO VCDs vs daily average Temperature in Field Campaign sites

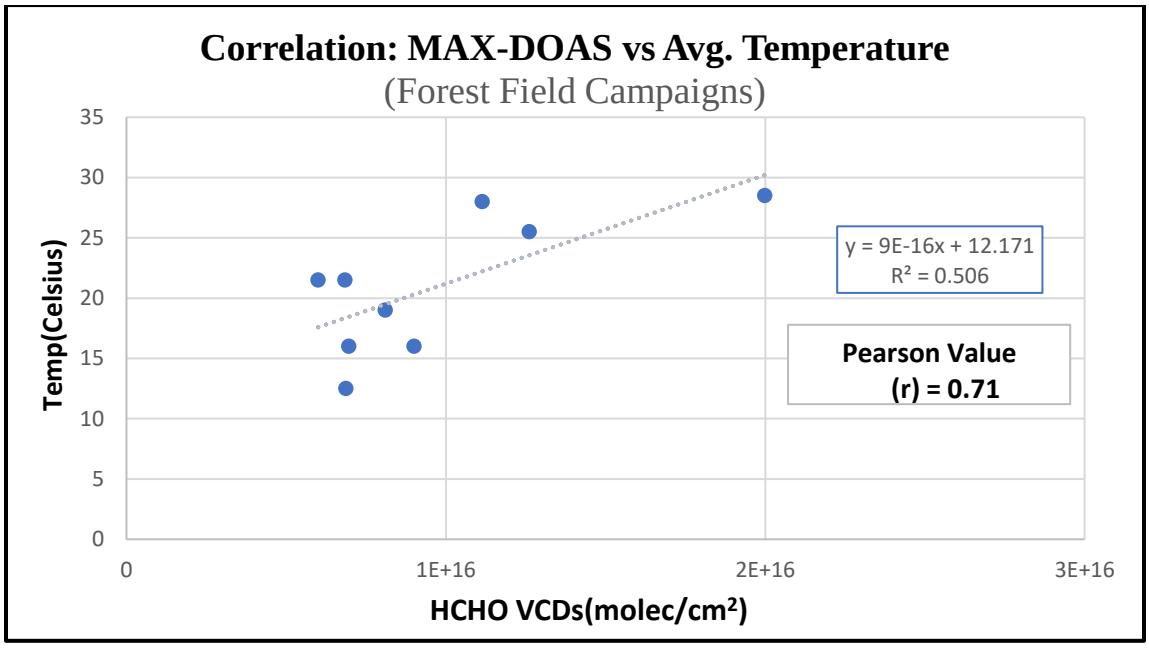

Figure 4. 25: Correlation of MAX-DOAS average HCHO VCDs vs daily average Temperature in Field Campaign sites

Chapter 5

5. Conclusions and Recommendations

5.1. Conclusions

HCHO mixing ratios measured during the study period of September, 2015- August, 2018 over IESE-NUST, Islamabad were found to be within the WHO threshold value of 83 ppbv. The HCHO diurnal cycle calculated for different seasons revealed that maximum concentrations were found during summer and minimum in winter mainly due to the lower temperature, OH production, lesser photolysis and lower biogenic emissions of VOCs in winter. The VCDs of HCHO were compared with temperature data over Islamabad and a correlation of 0.86 was found. While the NDVI values over IESE also showed positive correlation of 0.53 with the HCHO VCDs measured at IESE. HCHO VCDs were also compared with the industrial natural gas consumption as its supply and usage remains almost the same throughout the year while the supply and usage compressed natural gas for transportation and domestic use vary in winter and summer. CH_4 is a major source of HCHO and in our study, a correlation of 0.6 was found between HCHO VCDs and natural gas usage by industries in Islamabad.

Formaldehyde concentrations were found be within the WHO threshold value of 83 ppbv during the time period of forest field campaigns. The highest average VCD (1.9986E+16) was found in Tea Garden Shinkiari. The HCHO in the forest area was mainly contributed by the vegetation as temperature and HCHO VCDs showed a strong correlation of 0.71.

The forest campaigns were performed in summers and high temperature puts heat stress on plants and plants release HCHO precursors (NMVOCs) in response.

The mobile field campaigns in Lahore and Multan revealed that the HCHO concentrations were high near airport, industries and busy roads. The maximum concentration in Lahore city was found on 26th October 2018 (155.4 ppbv) that exceeded the WHO guideline (83 ppbv). The maximum concentration in Multan was found on 17th January 2019 (270.7.4 ppbv) which also exceeded the WHO guideline mainly due to congested traffic at that period of campaign.

Satellite data over IESE with the ground data showed correlation of 0.68 and 0.59 for comparison of both tropospheric and total column satellite data with ground-based results respectively. The satellite observations were observed to be underestimating the ground-based values.

5.2. Recommendations

Based on our findings, following are some of the recommendations for improving the air quality of Pakistan and promoting continuous air quality monitoring practices:

1. NEQs (National Environmental Quality Standards) should be formulated for HCHO concentrations in the ambient air.
2. Field Campaigns in forest areas of Pakistan should be conducted in each season of the year to generate database of air pollutants in these areas and also to investigate the seasonal trend.

3. Continuous air quality monitoring stations should be developed throughout the country for air quality assessment and effective pollution control techniques should be adopted for air pollution abatement.
4. Media campaigns should be run effectively for generating concern among the general public for air quality of the country.
5. Public should be given open access to air quality and health data by both government and non-government agencies.
6. Awareness among the school children, citizen groups etc. about air pollution, it's consequences and control should be spread for generating a sense of responsibility among them.
7. The use of mass transit system and adoption of other sustainable ways of transportation such as carpooling should be promoted in the mega-cities of the country.
8. Improved understanding of the production of HCHO precursors such as isoprene from vegetation is required through extensive and continuous monitoring.

6. References

Atkinson, R. (1997). Gas-phase tropospheric chemistry of volatile organic compounds: 1. Alkanes and alkenes. *Journal of Physical and Chemical Reference Data*, *26*(2), 215-290.

Ali, M., & Athar, M. (2008). Air pollution due to traffic, air quality monitoring along three sections of National Highway N-5, Pakistan. *Environmental monitoring and Assessment*, *136*(1-3), 219-226.

Baan, R., Grosse, Y., Straif, K., Secretan, B., El Ghissassi, F., Bouvard, V., ... & Cogliano, V. (2009). A review of human carcinogens—part F: chemical agents and related occupations. *The lancet oncology*, *10*(12), 1143-1144.

Brohede, S. (2002). Differential Optical Absorption Spectroscopy, How does it work and what can it measure?. *URL: http://home. elka. pw. edu. pl/~ rgraczyk/DOAS. pdf*.

Cantrell, C. A., Davidson, J. A., McDaniel, A. H., Shetter, R. E., & Calvert, J. G. (1990). Temperature-dependent formaldehyde cross sections in the near-ultraviolet spectral region. *Journal of Physical Chemistry*, *94*(10), 3902-3908.

Chen, W. T., Shao, M., Lu, S. H., Wang, M., Zeng, L. M., Yuan, B., & Liu, Y. (2014). Understanding primary and secondary sources of ambient carbonyl compounds in Beijing using the PMF model. *Atmospheric Chemistry and Physics*, *14*(6), 3047-3062.

Dickinson, R. E., & Cicerone, R. J. (1986). Future global warming from atmospheric trace gases. *nature*, *319*(6049), 109.

Fayt, C., & Van Roozendael, M. (2001). WinDOAS 2.1–Software user manual.*Uccle, belgium, bira-iasb*.

Fehsenfeld, F., Calvert, J., Fall, R., Goldan, P., Guenther, A. B., Hewitt, C. N., ... & Zimmerman, P. (1992). Emissions of volatile organic compounds from vegetation and the implications for atmospheric chemistry. *Global Biogeochemical Cycles*, *6*(4), 389-430.

Gratsea, M., Vrekoussis, M., Richter, A., Wittrock, F., Schönhardt, A., Burrows, J., ... & Gerasopoulos, E. (2016). Slant column MAX-DOAS measurements of nitrogen dioxide, formaldehyde, glyoxal and oxygen dimer in the urban environment of Athens. *Atmospheric environment*, *135*, 118-131.

Gouw, J. A., Gilman, J. B., Kim, S. W., Alvarez, S. L., Dusanter, S., Graus, M., ... & Lerner, B. M. (2018). Chemistry of volatile organic compounds in the Los Angeles Basin: Formation of oxygenated compounds and determination of emission ratios. *Journal of Geophysical Research: Atmospheres*, *123*(4), 2298-2319.

Guenther, A., Geron, C., Pierce, T., Lamb, B., Harley, P., & Fall, R. (2000). Natural emissions of non-methane volatile organic compounds, carbon monoxide, and oxides of nitrogen from North America. *Atmospheric Environment*, *34*(12-14), 2205-2230.

Guenther, A., Hewitt, C. N., Erickson, D., Fall, R., Geron, C., Graedel, T., ... & Pierce, T. (1995). A global model of natural volatile organic compound emissions. *Journal of Geophysical Research: Atmospheres*, *100*(D5), 8873-8892.

Ho, S. S. H., Ho, K. F., Lee, S. C., Cheng, Y., Yu, J. Z., Lam, K. M., ... & Huang, Y. (2012). Carbonyl emissions from vehicular exhausts sources in Hong Kong. *Journal of the Air & Waste Management Association*, *62*(2), 221-234.

Hönninger, G., Friedeburg, C. V., & Platt, U. (2004). Multi axis differential optical absorption spectroscopy (MAX-DOAS). *Atmospheric Chemistry and Physics*, *4*(1), 231-254.

Hoque, H. M. S., Irie, H., & Damiani, A. (2018). First MAX-DOAS Observations of Formaldehyde and Glyoxal in Phimai, Thailand. *Journal of Geophysical Research: Atmospheres*, *123*(17), 9957-9975.

Husain, T. (2010). Pakistan's Energy Sector Issues: Energy Efficiency and Energy Environmental Links. *Lahore Journal of Economics*, *15*.

ISAC, B. (1994). Differential optical absorption spectroscopy (DOAS).

Kampa, M., & Castanas, E. (2008). Human health effects of air pollution. *Environmental pollution*, *151*(2), 362-367.

Khan, F. I., & Ghoshal, A. K. (2000). Removal of volatile organic compounds from polluted air. *Journal of loss prevention in the process industries*, *13*(6), 527-545.

Kim, K. H., Jahan, S. A., & Lee, J. T. (2011). Exposure to formaldehyde and its potential human health hazards. *Journal of Environmental Science and Health, Part C*, *29*(4), 277-299.

Lee, M., Heikes, B. G., Jacob, D. J., Sachse, G., & Anderson, B. (1997). Hydrogen peroxide, organic hydroperoxide, and formaldehyde as primary pollutants from biomass burning. *Journal of Geophysical Research: Atmospheres*, *102*(D1), 1301-1309.

Levelt, P. F., van den Oord, G. H., Dobber, M. R., Malkki, A., Visser, H., de Vries, J., ... & Saari, H. (2006). The ozone monitoring instrument. *IEEE Transactions on geoscience and remote sensing*, *44*(5), 1093-1101.

Li, X., Brauers, T., Hofzumahaus, A., Lu, K., Li, Y. P., Shao, M., ... & Wahner, A. (2012). MAX-DOAS measurements of NO2, HCHO and CHOCHO at a rural site in Southern China. Atmos. Chem. Physics Discussion, 12(2), 3983-4029.

Liakakou, E., Vrekoussis, M., Bonsang, B., Donousis, C., Kanakidou, M., & Mihalopoulos, N. (2007). Isoprene above the Eastern Mediterranean: Seasonal variation and contribution to the oxidation capacity of the atmosphere. *Atmospheric Environment*, *41*(5), 1002-1010.

Luecken, D. J., Hutzell, W. T., Strum, M. L., & Pouliot, G. A. (2012). Regional sources of atmospheric formaldehyde and acetaldehyde, and implications for atmospheric modeling. *Atmospheric environment*, *47*, 477-490.

Marty, M., Spurlock, F., & Barry, T. (2010). Volatile organic compounds from pesticide application and contribution to tropospheric ozone. In *Hayes' Handbook of Pesticide Toxicology* (pp. 571-585). Academic Press.

Menezes, J. C. D., Borges, G. B. V., Gomes, F. D. C. O., Vieira, M. D. L. A., Marques, A. R., & Machado, A. M. D. R. (2019). Volatile compounds and quality analysis in commercial medicinal plants of Camellia sinensis. *Ciência Rural*, *49*(3).

Miller Jr, G. T. (1992). *Living in the environment: an introduction to environmental science* (No. Ed. 7). Wadsworth Publishing Company, Inc.

Nowak, D. J., Hirabayashi, S., Bodine, A., & Greenfield, E. (2014). Tree and forest effects on air quality and human health in the United States. *Environmental pollution*, *193*, 119-129.

Palmer, P. I., Jacob, D. J., Fiore, A. M., Martin, R. V., Chance, K., & Kurosu, T. P. (2003). Mapping isoprene emissions over North America using formaldehyde column observations from space. *Journal of Geophysical Research: Atmospheres*, *108*(D6).

Pachauri, R. K., & Reisinger, A. (2008). *Climate change 2007: Synthesis report. Contribution of Working Group II to the fourth assessment report of the Intergovernmental Panel on Climate Change*. Geneva, Switzerland: IPCC.

Ramanathan, V. C. P. J., Crutzen, P. J., Kiehl, J. T., & Rosenfeld, D. (2001). Aerosols, climate, and the hydrological cycle. *science*, *294*(5549), 2119-2124.

Salthammer, T. (2013). Formaldehyde in the ambient atmosphere: from an indoor pollutant to an outdoor pollutant?. *Angewandte Chemie International Edition*, *52*(12), 3320-3327.

Simon, V., Luchetta, L., & Torres, L. (2001). Estimating the emission of volatile organic compounds (VOC) from the French forest ecosystem. *Atmospheric Environment*, *35*, S115-S126.

Siwko, M. E., Marrink, S. J., de Vries, A. H., Kozubek, A., Uiterkamp, A. J. S., & Mark, A. E. (2007). Does isoprene protect plant membranes from thermal shock? A molecular dynamics study. *Biochimica et Biophysica Acta (BBA)-Biomembranes*, *1768*(2), 198-206.

Sprengnether, M., Demerjian, K. L., Donahue, N. M., & Anderson, J. G. (2002). Product analysis of the OH oxidation of isoprene and 1, 3-butadiene in the presence of NO. *Journal of Geophysical Research: Atmospheres*, *107*(D15), ACH-8.

Stavrakou, T., Müller, J. F., Bauwens, M., De Smedt, I., Van Roozendael, M., Guenther, A., ... & Xia, X. (2014). Isoprene emissions over Asia 1979–2012: impact of climate and land-use changes. *Atmospheric Chemistry and Physics*, *14*(9), 4587-4605.

Tian, X., Xie, P., Xu, J., Li, A., Wang, Y., Qin, M., & Hu, Z. (2018). Long-term observations of tropospheric NO2, SO2 and HCHO by MAX-DOAS in Yangtze River Delta area, China. *Journal of Environmental Sciences*, *71*, 207-221.

US Environmental Protection Agency. (1999). Integrated Risk Information System (IRIS) on Formaldehyde.

Vlasenko, A., Macdonald, A. M., Sjostedt, S. J., & Abbatt, J. P. D. (2010). Formaldehyde measurements by Proton transfer reaction–Mass Spectrometry (PTR-MS): correction for humidity effects. *Atmospheric Measurement Techniques*, *3*(4), 1055-1062.

Volkamer, R., Jimenez, J. L., San Martini, F., Dzepina, K., Zhang, Q., Salcedo, D., ... & Molina, M. J. (2006). Secondary organic aerosol formation from anthropogenic air pollution: Rapid and higher than expected. *Geophysical Research Letters*, *33*(17).

Vrekoussis, M., Wittrock, F., Richter, A., & Burrows, J. P. (2010). GOME-2 observations of oxygenated VOCs: what can we learn from the ratio glyoxal to formaldehyde on a global scale?. *Atmospheric Chemistry and Physics*, *10*(21), 10145-10160.

Watson, J. G., Chow, J. C., & Fujita, E. M. (2001). Review of volatile organic compound source apportionment by chemical mass balance. *Atmospheric Environment*, *35*(9), 1567-1584.

Wei, W., Wang, S., Chatani, S., Klimont, Z., Cofala, J., & Hao, J. (2008). Emission and speciation of non-methane volatile organic compounds from anthropogenic sources in China. *Atmospheric Environment*, *42*(20), 4976-4988.

Wilbur, S. B. (1999). *Toxicological profile for formaldehyde*. Atlanta, GA: U.S. Department of Health and Human Services, Public Health Service, Agency for Toxic Substances and Disease Registry.

Wuebbles, D. J., & Hayhoe, K. (2002). Atmospheric methane and global change. *Earth-Science Reviews*, *57*(3-4), 177-210.